Effective Date: 29 June 2022
Revision E

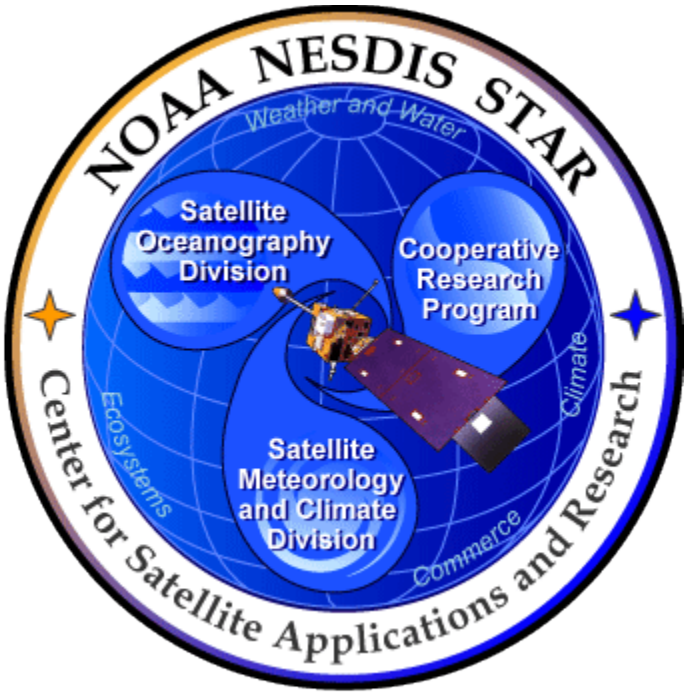

NOAA NESDIS
CENTER for SATELLITE APPLICATIONS and RESEARCH

Joint Polar Satellite System (JPSS) VIIRS Imagery Products Algorithm Theoretical Basis Document (ATBD)

Bill Line, NOAA/NESDIS/STAR
Don Hillger, NOAA/NESDIS/STAR
Thomas Kopp, Aerospace Corporation

https://www.star.nesdis.noaa.gov/jpss/Docs.php

TABLE OF CONTENTS

LIST OF FIGURES

LIST OF TABLES

ABSTRACT

This Imagery Algorithm Theoretical Basis Document (ATBD) describes the background, theory, and analysis of the algorithmic process required to create Imagery Environmental Data Records (EDRs) from the sensor Raw Data Records (RDRs) of the Joint Polar Satellite System (JPSS) Visible Infrared Imaging Radiometer Suite (VIIRS).

This document covers all VIIRS Imagery processing. In particular, it describes algorithms for producing explicit Imagery in the Ground-Track Mercator (GTM) projection. It also describes in detail the process to create Near Constant Contrast (NCC) Imagery from the Day Night Band (DNB) Sensor Data Records (SDRs).

The VIIRS instrument includes 6 bands defined as Imaging or I-bands. Each of these bands was chosen in the early stages of the National Polar-orbiting Operational Environmental Satellite System (NPOESS) program, the predecessor of JPSS, for explicit benefits in determining the presence of specific atmospheric or ground features, with an emphasis on clouds and sea ice. The VIIRS DNB was included to allow for a "visual" image under nighttime conditions. As the program progressed, it was determined a further set of Moderate (M-band) Imagery was also necessary. For each spectral band for which Imagery is provided, two data products are required. They are:

(a) A two-dimensional array of locally-averaged absolute in-band **radiances at the top of the atmosphere (TOA)**, measured in the direction of the viewing instrument, and
(b) The corresponding array of **Equivalent BlackBody Temperatures (EBBT)** if the band is primarily emissive; or the corresponding array of **top-of-the-atmosphere reflectances** if the band is primarily reflective in the daytime.

The VIIRS Imagery EDR benefits from true multispectral capability and compatibility with heritage from the Department of Defense (DoD) Defense Meteorological Satellite Program (DMSP) Operational Linescan System (OLS). The radiometric performance of the bands exceeds the specification for Measurement Uncertainty with margins that meet or approach objective requirements.

The explicit Imagery is computed from the VIIRS Sensor Data Records (SDRs) following the Build-SDR module, which applies geo-location, earth gridding, and calibration to the RDRs. The functionality of the Build-SDR module allows it to produce SDRs that fully meet the explicit Imagery requirements. All Imagery products are calibrated, geolocated, and reported for a set of earth locations forming an approximately rectangular lattice. The lattice spacing is 742 m +/- 5% for the DNB, and approximately equivalent to the Horizontal Spatial Resolution (HSR) for each other band.

NCC Imagery is derived from the DNB, and accounts for rapidly-changing solar or lunar illumination conditions that often increase the difficulty of a user to determine the feature they are seeking (i.e. clouds). The DNB is comprised of a three-stage Charge Coupled Device (CCD) to account for the wide-ranging reflectances from daytime to nighttime/new moon conditions. The dynamic range of the DNB covers approximately 7 orders of magnitude. The NCC algorithm uses

the DNB radiances and determines a pseudo-albedo by modeling the solar and lunar radiance for each pixel. The algorithm preserves heritage from the OLS Gain Management Algorithm (GMA) through the use of Look Up Tables (LUTs) designed to mimic the GMA. The resulting pseudo-albedos are then placed on the GTM projection.

A common use of Imagery is for cloud analysis. Manual cloud analysis is based upon the contrast, measured in brightness temperature or reflectance, between the cloud and the surrounding cloud-free background. In infrared (IR) imagery, cloud detection is enhanced not only by temperature contrasts between the features but also by observing the features in spectral bands where their emittance contrasts exist. In visible and near-infrared imagery, cloud detection relies on contrasts in the reflectances of the features while at mid-infrared wavelengths, e.g. 3-5 μm, both temperature and reflected solar energy can be exploited in the manual cloud analysis process. Image enhancement techniques such as histogram equalization and thresholding enable the analyst to delineate individual features. False-colored compositing of multispectral images facilitates manual interpretation of the clouds and background features by assigning colors to those pixels with different multispectral responses. Using these tools, the analyst can systematically and quickly identify and classify the various clouds in the imagery. A User's Guide (Seaman et al, 2015) has been developed as a separate document for those interesting in applications of the available VIIRS Imagery EDR.

Imagery is considered a Priority 1 requirement in the Joint Polar Satellite System (JPSS) Level 1 Requirements Document (L1RD). Additional requirements on Imagery are stated in the Level 1 Supplemental Document. Initially there were 6 bands required by the JPSS program to be applied as Imagery EDRs; they are bands I1, I4, I5, M14, M15, and M16. The focus for these requirements is for the Alaskan region, which receives inadequate Imagery support from standard geostationary satellites. Two additional bands were added later to this list, I3 and NCC. As of October 2020 all VIIRS bands are created as Imagery EDRs. I-band Imagery EDRs must have a spatial resolution of 400 m at nadir and 800 m at the edge-of-scan, while M-band and NCC Imagery are double those values (800/1600 m). These values are similar to the actual SDR spatial resolution for VIIRS (375 m for I-bands, 750 m for M-bands, and 742 m for DNB). The GTM projection as applied within the Interface Data Processing Segment (IDPS) meets or exceeds these requirements.

1 INTRODUCTION

1.1 Purpose

This Visible Infrared Imaging Radiometer Suite (VIIRS) Imagery Algorithm Theoretical Basis Document (ATBD) describes the processing steps required to create VIIRS Imagery Environmental Data Records (EDRs). It includes both a description of the Ground Track Mercator (GTM) projection and the process to produce Near Constant Contrast (NCC) Imagery from the VIIRS Day Night Band (DNB).

The early stages of VIIRS development included a focus on producing effective Imagery products. At that time three classes of Imagery requirements were used to aid in the design of VIIRS, they were: (a) explicit Imagery which included at least one daytime visible, one nighttime visible, and one infrared band, (b) application-related imagery, which identified Imagery bands needed to satisfy a minimum set of requirements for manually-generated cloud analysis and sea ice coverage, and (c) derived Imagery requirements derived to support other EDR requirements within the program. Although the concept of application-related requirements does not exist with the JPSS, the three principles above were the basis for the Imagery EDRs produced on the IDPS today.

Based on the principles above, the resulting Imagery algorithms were created to satisfy the following Imagery EDR processing functions:

(a) Generation of explicit Imagery EDRs from the Imaging (I-band) resolution.
(b) Creation of NCC visible Imagery from the DNB.
(c) Display VIIRS Imagery EDRs in the GTM projection.
(d) In addition, up to 6 Moderate (M-band) SDRs would also be included in the suite of Imagery EDRs available on the IDPS. In October 2020 the Imagery algorithm was extended to all M-bands.

1.2 Scope

All aspects of VIIRS Imagery processing are described in this ATBD. This section of the ATBD introduces the Imagery algorithms. Section 2 provides an overview of the Imagery EDR requirements and retrieval strategy. Section 3 describes the algorithm functions in detail, including the process flow, input data, theoretical basis, mathematical description, performance analysis, practical considerations, initialization, and validation. Section 4 states the assumption and limitations on which each algorithm is based. Section 5 provides references for the publications cited in this document.

Table 1 notes the sixteen (16) M bands, the five (5) I bands, and the DNB required as Imagery from the JPSS Level 1 Requirements Document (L1RD), as well as the associated spatial resolution requirements.

Table 1. Required Imagery EDR Products

Imagery EDR Product	VIIRS Band	Wavelength (μm)	Spatial Resolution Nadir/Edge-of-Scan
Visible/Reflective	I1	0.60 – 0.68	0.4 km/0.8 km
NIR	I2	0.846 – 0.885	0.4 km/0.8 km
SWIR	I3	1.58 – 1.64	0.4 km/0.8 km
MWIR	I4	3.55 – 3.93	0.4 km/0.8 km
LWIR	I5	10.5 – 12.4	0.4 km/0.8 km
Visible/Reflective	M1	0.402 – 0.422	0.8 km/1.6 km
Visible/Reflective	M2	0.436 - 0.454	0.8 km/1.6 km
Visible/Reflective	M3	0.478 - 0.488	0.8 km/1.6 km
Visible/Reflective	M4	0.545 – 0.565	0.8 km/1.6 km
Visible/Reflective	M5	0.662 - 0.682	0.8 km/1.6 km
NIR	M6	0.739 - 0.754	0.8 km/1.6 km
NIR	M7	0.846 - 0.885	0.8 km/1.6 km
SWIR	M8	1.23 - 1.25	0.8 km/1.6 km
SWIR	M9	1.371 – 1.386	0.8 km/1.6 km
SWIR	M10	1.58 - 1.64	0.8 km/1.6 km
SWIR	M11	2.23 - 2.28	0.8 km/1.6 km
MWIR	M12	3.61 - 3.79	0.8 km/1.6 km
MWIR	M13	3.97 - 4.13	0.8 km/1.6 km
LWIR	M14	8.4 – 8.7	0.8 km/1.6 km
LWIR	M15	10.263 – 11.263	0.8 km/1.6 km
LWIR	M16	11.538 – 12.488	0.8 km/1.6 km
NCC	DNB	0.5 – 0.9	0.75 km/0.75 km

Of the twenty-two (22) VIIRS bands, the eight (8) VIIRS bands with text highlighted in yellow in Table 1 are considered to be VIIRS Key Performance Parameters (KPPs) for latitudes greater than 60°N in the Alaskan region.

1.3 Revisions

This is Revision E to the VIIRS Imagery Products ATBD. This update corresponds to the implementation of all VIIRS M-bands being created as Imagery EDRs. This ATBD now aligns with the Imagery Software Requirements Specification (SRS), the Imagery Data Description (DD) document, the Level 1 Requirements Document (L1RD) and the Ground Segment Data Product Specification (GSegDPS) documents.

Revision D corresponds to the transition from Imagery on the Ellipsoid to that of Terrain Corrected (TC) Imagery. This change was mandated by an updated set of requirements, including one labeled "TC-IMG-R 4.0" which states, "The TC Imagery (TC-IMG) Processing System (PS) shall generate the JPSS VIIRS EDR (M-band, I-band, and NCC) Terrain-Corrected Imagery products."

Two Configuration Change Requests (CCR) accompanied this task: CCR 8239 originated the effort to move Imagery EDRs to TC output; and CCR 8656 covered the software updates necessary within the geolocation software suite to accomplish TC Imagery. Section 3.5 covers the TC impact on the Imagery EDRs.

Revision C to the VIIRS Imagery Products ATBD corresponds to the work achieving the Provisional Stage of the Imagery EDR for NOAA-20 (JPSS-1). The major modification from Revision B is the inclusion of M-band Imagery products and replacing prior references to the now defunct NPOESS with current JPSS documentation. Prior discussion on application-related requirements was removed as they no longer exist. The former Appendix A was also removed, as that is now covered by a separate Imagery EDR User's Guide (Seaman et al, 2015). Consistency with other JPSS documents also forced numerous changes throughout this ATBD.

Revision B of the VIIRS Imagery Product ATBD was required to address actions identified by audits made in preparation for the VIIRS Critical Design Review (CDR). The major modification required in this update was a discussion of the procedures used to transform VIIRS Imagery into the GTM projection. In addition, procedures and automated algorithms used to support the manually-generated cloud and sea ice Application Related Products (ARPs) were highlighted since these processes are covered in other reports.

Revision A of this document was the initial release to bring it into Matrix Accountability. Prior to this, all versions were based upon naming conventions used by Raytheon, the originally developer of this ATBD. In that series of updates, Version 5.1 revision 2, made three changes to the document. First, bands I2 and I3 are now included as Imagery EDR bands, per the NPOESS system specification, and references to these two additional bands were added throughout the document. Also, the mathematical description added some equations to clarify the theory and explain the relationship between the theory and the LUTs in the algorithm. Finally, in Section 3.3.5.2 describing the atmospheric correction enhancement, additional text was added to indicate that changes to the algorithm would be necessary to implement aerosol scattering removal if deemed desirable. Text was added to consider the benefits of removing Rayleigh atmospheric effects without removing aerosols.

2 EXPERIMENT OVERVIEW

2.1 EDR Definition

As noted in Section 1.1, the VIIRS Imagery requirements initially fell into three classes, and these continue to be guiding principles in the creation of appropriate algorithms. The three principles are: (a) explicit Imagery which includes at least one daytime visible, one nighttime visible, and one infrared band; (b) application-related imagery, which identified Imagery bands needed to satisfy a minimum set of requirements for manually-generated cloud analysis and sea ice coverage, and (c) derived Imagery requirements derived to support other EDR requirements within the program. It is from this point that explicit Imagery requirements may be discussed.

2.2 Explicit Imagery Requirements

The original NPOESS System Specification precisely defined Imagery as providing two data products. Although not explicitly spelled out by the JPSS program, the content of the Imagery EDR retains delivering Imagery with both data products embedded. They are:

(a) A two-dimensional array of locally-averaged absolute in-band **radiances at the top of the atmosphere (TOA)**, measured in the direction of the viewing instrument, and
(b) The corresponding array of **Equivalent BlackBody Temperatures (EBBT)** if the band is primarily emissive; or the corresponding array of **top-of-the-atmosphere reflectance** if the band is primarily reflective in the daytime.

The local averages are reported for the points of a two-dimensional approximately rectangular lattice. The form of the weighting function that determines the local average (pixel aggregation) is constrained by the horizontal spatial resolution requirement. Data collected by the VIIRS I-bands are characterized by a horizontal spatial resolution of 375 m at nadir from a nominal altitude, while those from M-bands are at 750 m. The DNB is a special case, since it was intended to mimic the OLS day/night visual band. Its resolution is approximately 742 m but remains close to that resolution even towards the edge-of-scan. From an Imagery EDR point-of-view however, the DNB is mapped to the same GTM as that for M-bands, to ease NCC use as a component in a multispectral image. Other important derived requirements, in addition to those noted in Table 1, include:

1) The NCC Imagery EDR must minimize the apparent transition across the terminator.
2) All VIIRS Imagery EDRs shall be produced on the GTM projection.
3) The VIIRS Imagery EDR shall provide a mapping from the resultant projected VIIRS Imagery EDR geolocation to the source VIIRS SDR geolocation.

The latter requirement allows any user or those validating Imagery to determine the exact source of the original pixel that contributed to the associated value (radiance/reflectance/EBBT) within the corresponding Imagery EDR.

Table 2 compares the VIIRS bands supporting the Imagery ATBD with the bands from the OLS and with the European version of the Advanced Very High Resolution Radiometer (AVHRR-3).

Table 2. Comparison of VIIRS Imagery EDR bands with OLS and AVHRR

VIIRS			AVHRR-3 Equivalent			OLS Equivalent		
VIIRS Band	Spectral Range (μm)	Nadir HSR (m)	Band	Range	Nadir HSR (m)	Band	Range	Nadir HSR (m)
DNB	0.500 - 0.900					PMT	0.510 - 0.860	2700
						HRD	0.580 - 0.910	550
M1	0.402 - 0.422	750						
M4	0.545 - 0.565	750						
I1	0.600 - 0.680	375	1	0.572 - 0.703	1100			
I2	0.846 - 0.885	375	2	0.720 - 1.000	1100			
M9	1.371 - 1.386	750						
I3	1.580 - 1.640	375	3a	1.628 - 1.652	1100			
I4	3.550 - 3.930	375	3b	3.550 - 3.930	1100			
M14	8.400 - 8.700	750						
M15	10.263 - 11.263	750	4	10.300 - 11.300	1100			
I5	10.500 - 12.400	375	4	10.300 - 11.300	1100	HRD	10.300- 12.900	550
M16	11.538 - 12.488	750	5	11.500 - 12.500	1100			

2.3 NCC Imagery

The Imagery EDR includes a daytime/nighttime visible Imagery product that maintains apparent contrast under daytime, nighttime, and terminator region illumination conditions. This product is referred to as NCC Imagery. It is derived from the DNB, specifically the calibrated DNB radiance. The design of the NCC process/algorithm was initially based on five derived requirements, which were:

1) The NCC Image EDR shall minimize the apparent transition across the terminator when it is viewed on a graphical display system. This means, that from the perspective of a human analyst viewing the imagery, the apparent image contrast is maintained across the Imagery granule, and that there are no spatial or other artifacts which adversely affect the utility of the imagery.

2) The HSR of the NCC Imagery EDR shall meet the HSR of the Moderate (M-band) visible band Imagery EDR
3) The Horizontal Resolution Interval (HRI) of the NCC Imagery EDR shall be constant to within 5% of its nominal value in both the in-track and cross-track directions. Note this requirement is met by the use of the GTM projection.
4) The nominal value of the HRI of the NCC Imagery EDR shall provide gapless or near-gapless coverage based on the minimum HSR in either the in-track or cross-track directions along the Imagery swath.
5) The NCC Imagery EDR shall be geolocated by ground processing to meet the uncertainty requirement.

2.4 Ground-Track Mercator (GTM) Imagery

All VIIRS Imagery EDRs shall be projected onto a GTM layout. The GTM layout is a grid of pixels, where rows are at right angles to the ground track and columns are parallel to the ground track. The Imagery EDR are products designed for display and human viewing, and do not directly feed any downstream VIIRS EDR. Greater detail on the creation of GTM may be found in Section 3.4.

2.5 Instrument Characteristics

The VIIRS instrument can be pictured as a convergence of three existing sensors. (1) The OLS is the operational visible/infrared scanner for the DoD. Its unique strengths are controlled growth in spatial resolution through rotation of the Ground Instantaneous Field Of View (GIFOV) and the existence of a Low Level Light Sensor (LLLS) capable of detecting visible radiation at night. OLS has primarily served as a data source for manual analysis of imagery. (2) The AVHRR is the operational visible/infrared sensor flown on the NOAA Television InfraRed Observation Satellite (TIROS-N) series of satellites (Planet, 1988). Its unique strengths are low operational and production cost and the presence of 6 spectral bands that can be used in a wide number of combinations to produce operational and research products. (3) The Moderate Resolution Imaging Spectroradiometer (MODIS) which possesses an array of 36 spectral bands at resolutions ranging from 250 m to 1 km at nadir.

The original design of VIIRS intended to merge and extend the capabilities of each of these three sensors while meeting numerous requirements under the prior NPOESS program. As such, VIIRS includes key attributes of high spatial resolution with controlled growth off nadir and a large number (22 in all) of spectral bands. A relatively brief description of the design concept, scanning method, and pixel formation for VIIRS is given in Section 3.2.5, however readers interested in further detail may peruse the VIIRS SDR ATBD.

The requirements for Imagery played a major role in the design of the VIIRS instrument. The I-bands, as shown in Table 1, contain characteristics that were primarily driven by the expected use of VIIRS Imagery products. Within the prior NPOESS program, the Imagery needs were

defined first, and only after that were the SDR requirements derived. In the early stages it was believed all of the Imagery requirements could be met through the I-bands and DNB only, hence all M-band SDR requirements were derived for other purposes. As the program evolved, it was evident further assistance for Imagery users would exist if certain M-bands were also available as an Imagery product. After extensive discussions, with consideration for resource constraints, the program decided to add the capability to create 6 M-bands as Imagery prior to the launch of SNPP. With time and use the value of Imagery from the other bands became evident, and by October 2022 all M-bands were produced as Imagery EDRs. Three of those were identified as important enough to now be required by JPSS (M14, M15, and M16) as noted in Table 1.

The current radiometric performance of VIIRS exceeds the specifications for Measurement Uncertainty, with sufficient margin that VIIRS Imagery has proven useful in determining a large number of atmospheric and ground features. These capabilities are discussed in the Imagery EDR User's Guide (Seaman et al, 2015). The following sections give insight to the reader on the selection and purpose of the I-bands and DNB, which as indicated above were selected specifically to support Imagery products.

2.5.1 DNB Instrument Characteristics

The DNB was an explicit requirement in the prior NPOESS, in part as a replacement for the OLS. Its design however, results in performance that exceeds the OLS, if for any other reason than the DNB is part of a radiometer and the OLS is only an imager.

DNB data is taken by a sensitive, very-wide-dynamic range CCD detector in the main VIIRS sensor. The CCD is located adjacent to the Visible/Near InfraRed (VNIR) detector chip on the Warm Focal Plane. It is positioned so that as the sensor scans the image of the Earth across the focal plane, a particular point on earth is imaged first by the VNIR chip and then by the DNB CCD.

The detective elements of the DNB CCD are 15.4 μm by 24.2 μm photosites. In the VIIRS sensor each of these photosites images an angle that corresponds to approximately 17 x 11 m on the ground at nadir. The signals from many of these photosites are combined on the CCD chip to create the analog signals corresponding to entire ground pixels.

To encompass the extreme radiometric dynamic range of day and night scenes, the DNB CCD includes four regions of light-sensitive photosites with three different sensitivities:

Most Sensitive Regions: The CCD includes 2 identical regions incorporating 250 subpixel detectors operated in Time Delay Integration (TDI) mode. This TDI gives a total effective integration period 250 times longer than the integration period of a single subpixel detector, and thus increases sensitivity by approximately 250 times. In normal circumstances the signals from these two identical maximum-sensitivity detector regions are added together for further improvement in Signal-to-Noise Ratio (SNR). However, if radiation should compromise the value of a pixel measurement made by one of the two segments, the corresponding pixel signal from the other segment would be used.

Medium-sensitivity region: A second detecting region on the CCD chip utilizes three subpixel detectors in TDI. This region also has a lower amplifier gain to give it a net radiometric gain that is approximately 200 times less than the gain of the most sensitive regions.

Lowest-sensitivity region: The CCD also incorporates a detecting region that does not incorporate multiple detectors in TDI. In addition, this region incorporates a 35:1 neutral density filter and reduced amplifier gain, resulting in a radiometric gain approximately 1/475 of the medium-sensitivity region's gain.

The three regions are designed so that before a more sensitive region saturates, the next less sensitive region will have received a signal sufficient to produce an acceptable SNR. Analog signals from all three regions are converted into digital form and processed digitally to select the signal from the region offering the best SNR for each pixel.

The CCD design allows a variable number of subpixel elements to be aggregated into single pixels as they are read from the CCD. In the VIIRS sensor this capability is used to generate pixels with near-rectangular sample spacing on the ground. To accomplish this, many different aggregation modes are used during the course of the crosstrack sensor scan. Since the subpixel aggregation is an additive process, the total number of subpixels aggregated to create each pixel appears as a factor in the radiometric gain of the pixel.

2.5.2 VIIRS Imagery Band Selection Process

Band selection for the VIIRS sensor was based upon the strength (strong and/or weak) of three components that make up the signatures of each feature. These components were: (a) surface radiance which includes temperature and emittance or surface reflectance, (b) cloud absorptivity or reflectance, and (c) atmospheric transmissivity. An example of these features covering the SWIR spectrum is shown in Figure 1.

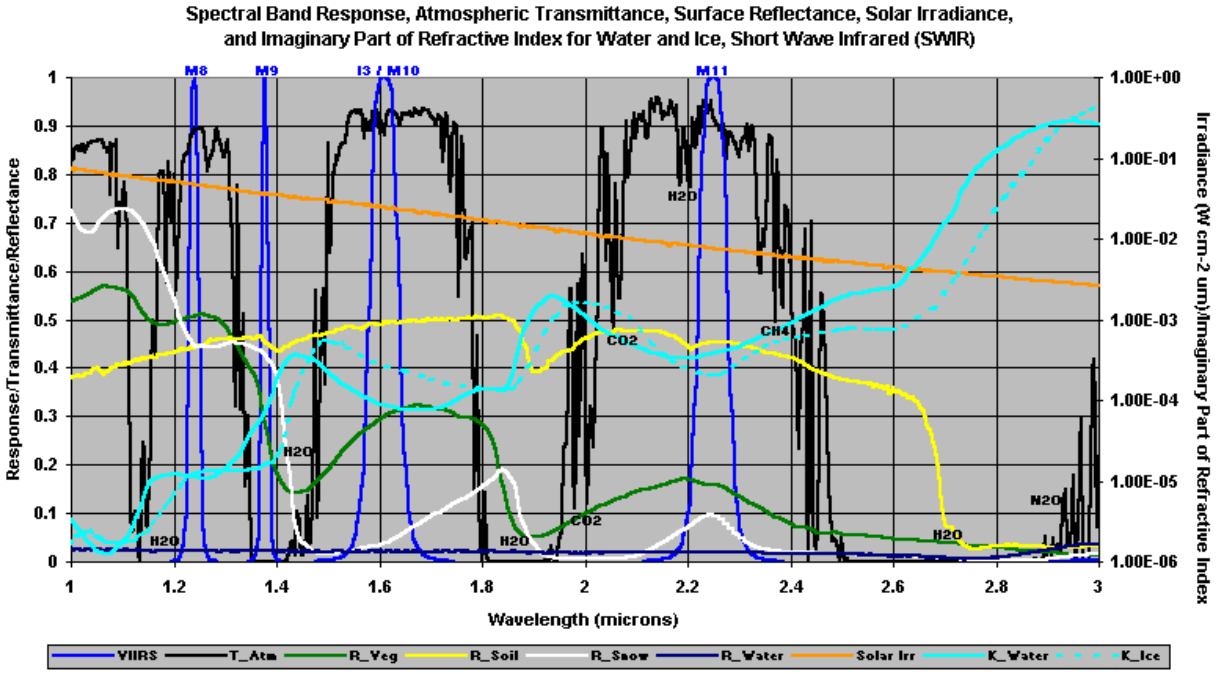

Figure 1. Reflectivity, absorptivity, and transmissivity of atmosphere, surface, and clouds in the Short-Wave InfraRed (SWIR).

Figure 1 shows the band positions for VIIRS bands M8, M9, I3/M10, and M11 (dark blue) along with atmospheric transmissivity (black), reflectivity of vegetated (green) and bare soil (yellow) ice (white) and water surfaces (blue), solar irradiance (gold), and imaginary components of the index of refraction for water (**light blue/solid**) and ice (light blue/dashed). This format is used for the following sections on each of the I-bands.

The positive identification of clouds in multispectral Imagery requires that the analyst understand and exploit the properties of water droplets and ice crystals, along with the spectral characteristics of different backgrounds in VIIRS Imagery EDRs. Clouds, along with sea ice, were major considerations in the establishment of the I-bands ultimately selected.

2.5.3 Visual Bands

Figure 2 shows the wavelength location and logic behind band I1. The entire visual spectrum is shown so the reader may also identify bands I2 and the M-bands from M1 to M7 (see Table 1), which are among the additional 6 M-bands available as an Imagery EDR.

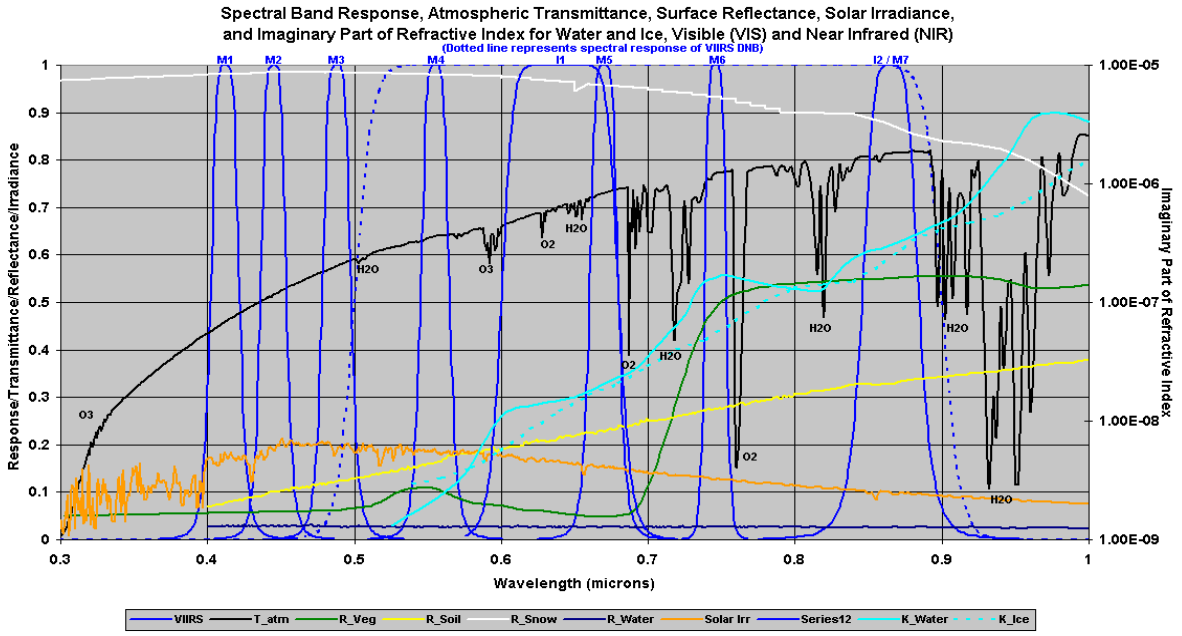

Figure 2. Phenomenology of the VIIRS Visible Bands

Figure 2 shows the location and spectral response function for the VIIRS visual bands, along with the characteristics of the Earth-atmosphere system. Focusing on band I1, it is clear that the reflectance of vegetated land is very small in this band but it begins to increase quite rapidly at ~0.7 µm. By limiting the longwave response of the band to <0.7 µm, we also avoid the water vapor absorption lines in the 0.7-0.8 µm region which could cause variations in cloud and land signatures. The reflectance of water surfaces is even lower. On the other hand, the reflectance of clouds is much larger which means this band is particularly valuable for discriminating between clouds and vegetated land and ocean surfaces. Additionally, the reflectance of snow is very high. Therefore, this band is not good for differentiating between snow and clouds nor is it particularly useful for identifying boundaries between land and ocean surfaces. Bands M1 through M4 are similar in that they reflect little radiation with vegetation or bare soil within their respective wavelengths.

2.5.4 Long-Wave InfraRed (LWIR) Bands

At least one LWIR band was required to among those available as an Imagery EDR. Band I5 was chosen; based both on historical usage and multispectral possibilities with other chosen I-bands. When the later discussion on adding M-band Imagery occurred, it was agreed all of the three M-bands in the LWIR portion of the spectrum would have a benefit, and this evolved into the JPSS requirement that all three are now required Imagery EDRs as well. Figure 3 shows the location and spectral response for all of these LWIR bands.

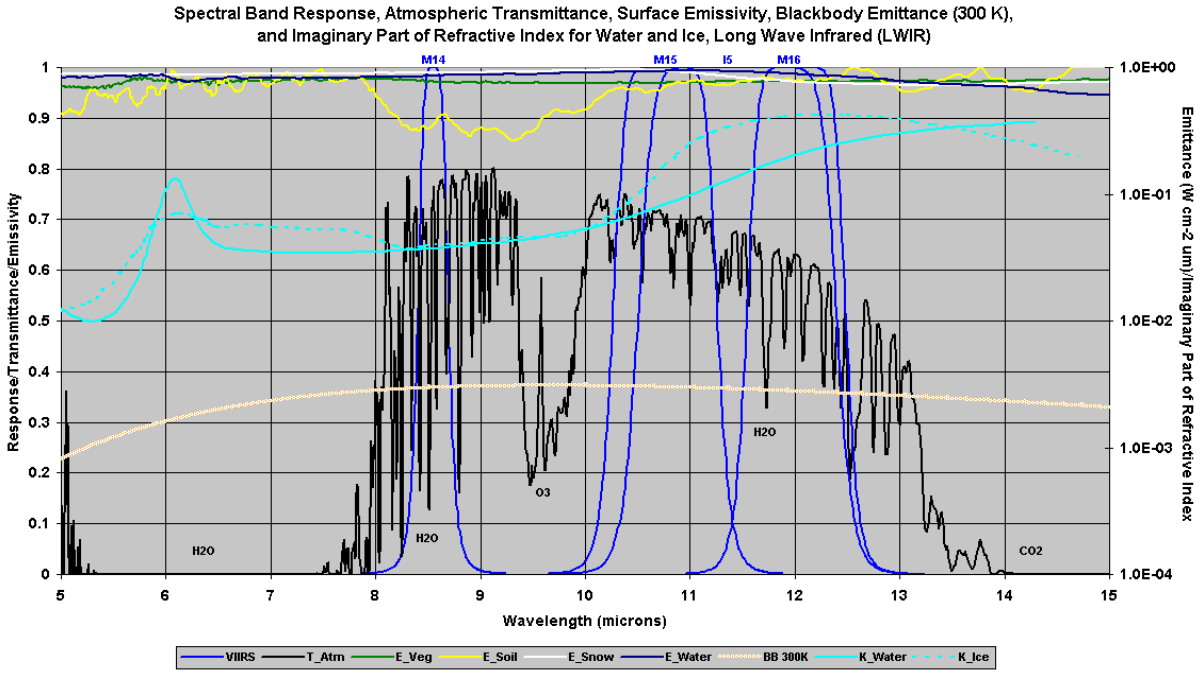

Figure 3. Phenomenology of the VIIRS LWIR Bands

Figure 3 includes the water vapor absorption across the LWIR spectrum. These bands in general are valuable for estimating the true radiating temperature of objects in the band after correcting for water vapor attenuation, which if not accounted for would indicate a cloud top temperature colder than reality. In addition, due to the high absorptivity of ice at these wavelengths, thin cirrus is often more easily detected. Band M14, in combination with the other LWIR bands, has also been found useful in determining cloud phase.

2.5.5 Mid-Wave InfraRed (MWIR) Bands

The flow down of requirements for VIIRS quickly identified the necessity to include a MWIR band among those created as an Imagery EDR. Heritage use from AVHRR supported the decision to include a MWIR band among the I-bands to exist on VIIRS. Figure 4 shows the MWIR bands on VIIRS, including band I4.

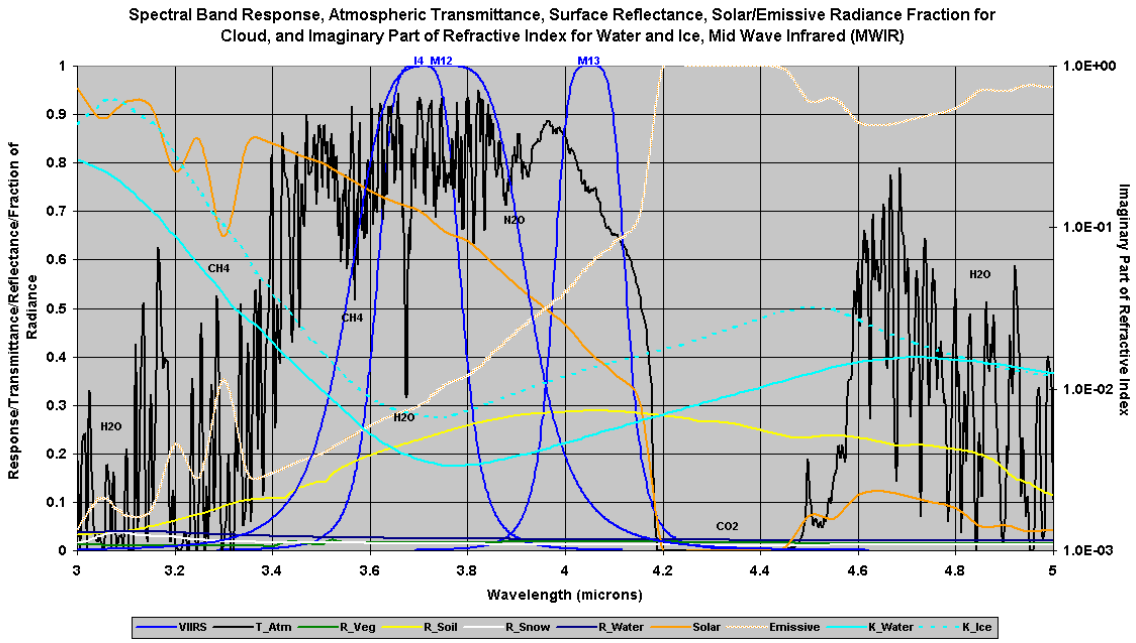

Figure 4. Phenomenology of the VIIRS MWIR Bands

Figure 4 includes the absorptions lines in the MWIR portion of the spectrum. The reflectance of snow is low in this region, while clouds are much larger. Considerable solar irradiance is present at wavelengths below approximately 4.2 µm, while the reflectance of bare soil is relatively large compared to snow and vegetation. Therefore, I4 can be useful for differentiating between snow and clouds as well as clouds and vegetated land. However, distinctions between clouds and bare soil are more difficult and the presence of terrestrial energy complicates the contrast between snow and clouds. As noted in the Imagery EDR User's Guide (Seaman et al, 2015), MWIR bands are quite useful in spotting low clouds at night, where the cloud top temperature may be similar to the surface.

2.5.6 Additional Imagery Bands

The first set of Imagery EDRs comprised those derived from the SDRs of bands I1, I4, I5, and the DNB. Guided by the initial focus on determining Imagery most favorable for locating clouds and sea ice, two additional I-bands were chosen. I2, shown in Figure 2, was added primarily to assist the cryosphere community locate sea ice edges. I3, shown in Figure 1, was chosen since it has proven to be an excellent discriminator between snow/ice and clouds. Figure 1 indicates ice contains a very low reflectance in the vicinity of 1.6 µm. Water clouds become quite distinguishable from snow/ice backgrounds due to this characteristic for band I3.

In the mid-2000s time frame, significant debates arose on whether or not the Imagery EDRs planned at that time (I1 through I5 plus NCC) were sufficient for users to determine the features of interest applicable to them. Imagery users, beyond those for clouds and sea ice, expressed a desire for more VIIRS bands to become available as an Imagery EDR. Resource constraints at

that time prevented the program from committing to all 16 M-bands, and a compromise of 6 M-bands was reached. They were M1, M4, M9, M14, M15, and M16. By 2020 all M-bands are configurable on the IDPS, and today all M-bands are now available as Imagery EDRs. The use of the LWIR bands among the Alaskan National Weather Service (NWS) also resulted in JPSS now requiring certain M-bands bands as part of the Imagery EDR suite of products.

2.6 Retrieval Strategy

2.6.1 Explicit imagery

The necessary VIIRS SDRs are produced from the VIIRS Raw Data Records (RDRs) by a RDR-to-SDR conversion algorithm. They are produced as pixels separated by a HRI. The process of sampling and aggregation achieves a roughly HRI equivalent to the HSR. Details of this process may be found in the VIIRS SDR ATBD.

2.6.2 Top-of-Atmosphere Radiance

Calibrated Top-of-Atmosphere (TOA) radiance from all bands is produced in the Build-SDR module. A short overview of this process is given in Section 3.2.1, but further details may be found in the VIIRS Radiometric Calibration ATBD.

2.6.3 Top-of-Atmosphere Reflectance

Digital numbers in the visible bands, to include the DNB, are first converted to radiances, but then further converted into TOA reflectances. Note the NCC Imagery EDR, produced from the DNB SDRs, is further converted into pseudo-albedos. However all other visual Imagery products retain reflectances (they also retain the radiance values). The process of determining reflectances is described in the VIIRS SDR ATBD and VIIRS SDR User's Guide (Cao et al, 2014). The NCC algorithm is described in Section 3.3.

2.6.4 EBBT

Digital numbers in the MWIR and LWIR bands first become radiances, then are converted to EBBTs. This process is also described in the VIIRS SDR ATBD and associated SDR User's Guide (Cao et al, 2014).

3 ALGORITHM DESCRIPTION

3.1 Overview

The Imagery algorithm, other than that for NCC Imagery, comprises the logic necessary to place radiances/reflectances/EBBTs onto the GTM layout. The NCC process includes the creation of pseudo-albedos, which are determined before the transition to GTM. This section describes both processes. Since there are certain characteristics of VIIRS relevant to Imagery users, these aspects of the sensor are described in this section as well.

3.2 Explicit Imagery Production

3.2.1 Processing Outline

VIIRS SDRs are computed from the VIIRS RDRs, as part of the Build-SDR module, which applies geolocation and calibration to the RDRs. The functionality of the Build-SDR module allows it to produce SDRs which fully meet the explicit Imagery requirements. The VIIRS I-band SDRs contain the TOA radiance for bands I1, I2, I3, I4, and I5, the TOA reflectance for bands I1, I2, and I3, and EBBT for bands I4, and I5, with associated geolocation and band quality flags. Likewise M-band SDRs contains the necessary data for M-band Imagery EDRs and the DNB SDR contains those required for NCC Imagery. The Imagery algorithm obtains this data, and includes it in the output Imagery EDR file.

3.2.2 Algorithm Input

The SDR algorithm requires the VIIRS RDRs for each Imagery band. These RDRs are created by the ingest function of the IDPS. At this stage no other inputs are required. The Imagery EDR requires only information with the SDRs, associated geolocation output, and the spacecraft diary. The latter is used to create the GTM. No non-VIIRS data is necessary to create VIIRS Imagery EDRs.

3.2.3 Archived Algorithm Output

Like all other delivered products from the IDPS, the Imagery EDRs are stored in a HDF5 format. All Imagery EDRs are geolocated and contain their own geolocation file. However, only the I-band Imagery and NCC Imagery EDRs are archived in long term storage systems such as the Comprehensive Large Array-data Stewardship System (CLASS). M-band Imagery may be found on GRAVITE for up to 34 days after its creation, but these Imagery products are not archived for long term use. RDRs may be found on GRAVITE for up to 90 days, from which the Imagery SDRs and EDRs can be re-created using appropriate offline processing such as the NOAA JPSS-funded Community Satellite Processing Package (CSPP).

3.2.4 VIIRS Imaging Band Characteristics

Imagery is created after obtaining the appropriate SDRs, to include the DNB. The SDRs are obtained from VIIRS RDRs by an RDR to SDR process. The RDRs are obtained by a rotating telescope scanning mechanism that minimizes the effects of solar impingement and scattered light. Figure 5 illustrates the design concept for VIIRS, designed and built by Raytheon Santa Barbara Remote Sensing (SBRS). Calibration is performed onboard using a solar diffuser for short wavelengths and a blackbody source and deep space view for thermal wavelengths. A Solar Diffuser Stability Monitor (SDSM) is also included to track the performance of the solar diffuser. The VIIRS scan extends to 56 degrees on either side of nadir, providing a swath of >3000 km for the nominal satellite altitude of 833 km.

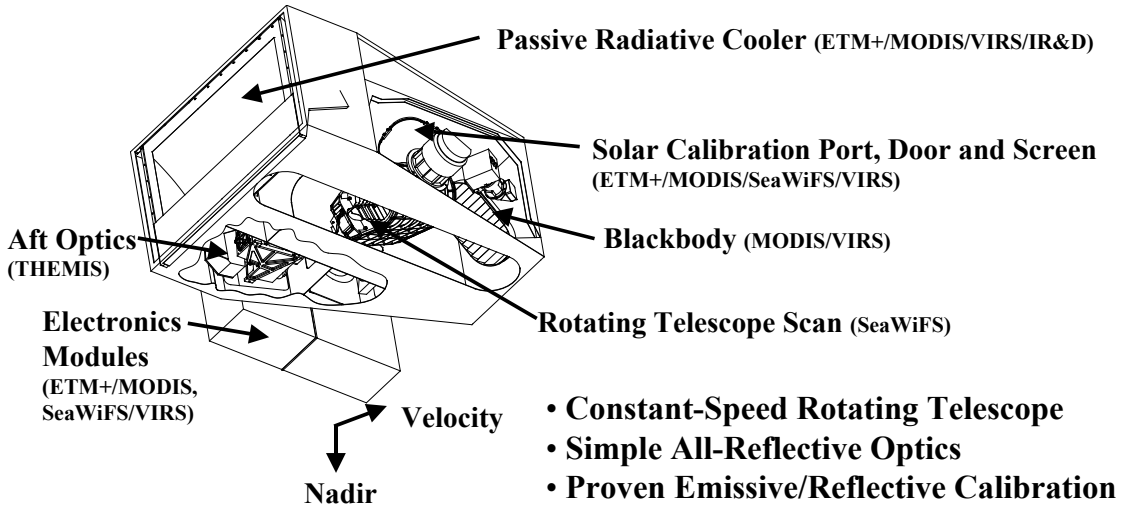

Figure 5. Summary of VIIRS design concepts and heritage

The explicit spatial resolution requirements on the VIIRS SDRs were derived initially from requirements placed on the Imagery EDRs. Specifically, the HSR of bands used to meet threshold Imagery EDR requirements must be no greater than 400 m at nadir and 800 m at the edge of the scan (I-bands). This led to the development of a unique scanning approach which optimizes both spatial resolution and SNR across the scan. The concept is summarized in Figure 6 for the I-bands. The VIIRS detectors are rectangular, with the smaller dimension along the scan. At nadir, three detector footprints are aggregated to form a single VIIRS "pixel." Moving along the scan away from nadir, the detector footprints become larger both along track and along scan, due to geometric effects and the curvature of the Earth. The effects are much larger along scan. At 31.59 degrees in scan angle, the aggregation scheme is changed from 3x1 to 2x1. A similar switch from 2x1 to 1x1 aggregation occurs at 44.68 degrees. The VIIRS scan consequently exhibits a pixel growth factor of only 2 both along track and along scan, compared with a growth factor of 6 along scan which would be realized without the use of the aggregation scheme. This scanning approach allows VIIRS to provide Imagery at 800 m resolution or finer globally, with 375 m resolution at nadir. Additionally, due to the Imagery requirements for VIIRS and the "sliver" detector design, Modulation Transfer Function (MTF) performance is extremely sharp (0.5 at Nyquist).

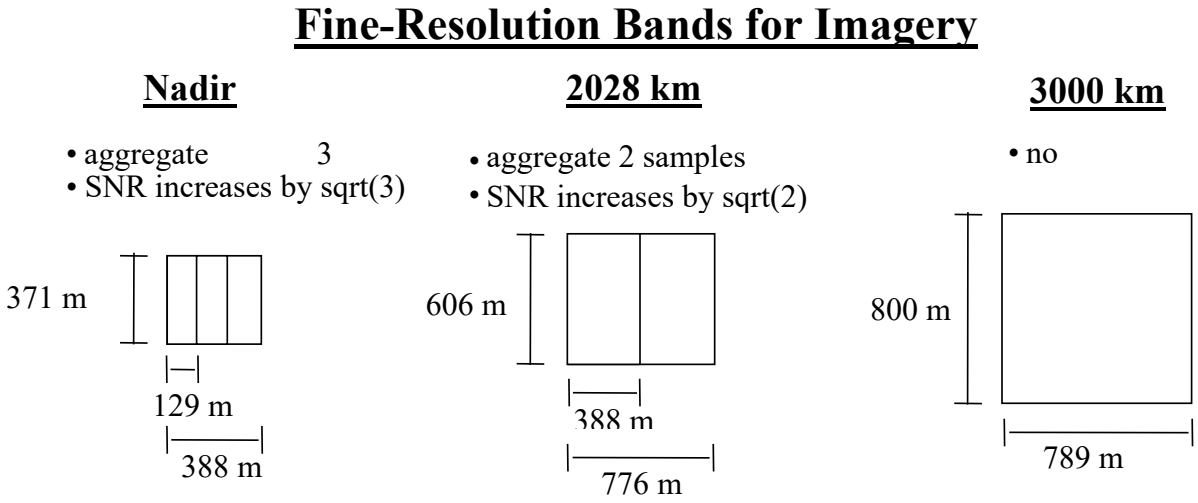

Figure 6. VIIRS detector footprint aggregation scheme for building Imagery "pixels

Figure 7 shows the resulting Horizontal Sampling Interval (HIS) from the combination scan/aggregation scheme.

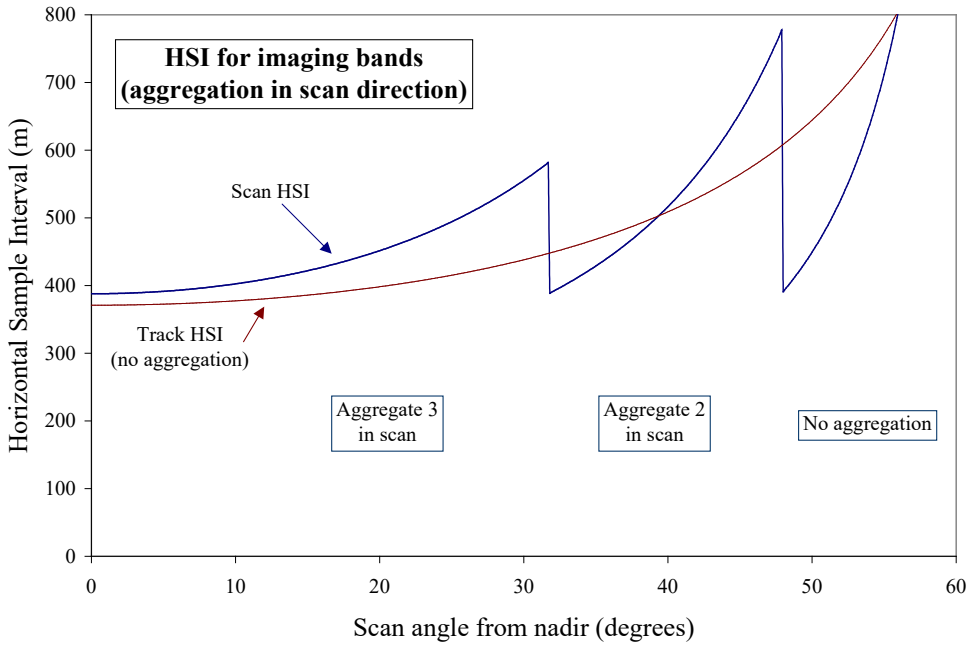

Figure 7. Horizontal Sampling Interval for I-bands (aggregation in scan direction)

The HRI of the Imagery is that of the Horizontal Sampling Interval (HIS). The MTF specification of 0.5 at the sampling Nyquist frequency results in a HSR equal to the HSI.

Even though the aggregation scheme greatly reduces the growth in HSI across the scan, there is still a factor of 2 growth resulting in a residual "bowtie" effect. An additional reduction in the bowtie effect is achieved by deleting 4 of the 32 detectors from the output data steam for the middle (Aggregate 2) part of the scan and 8 of the 32 detectors for the edge (No aggregation) part of the scan. Figure 8 illustrates the resultant additional bowtie deletion.

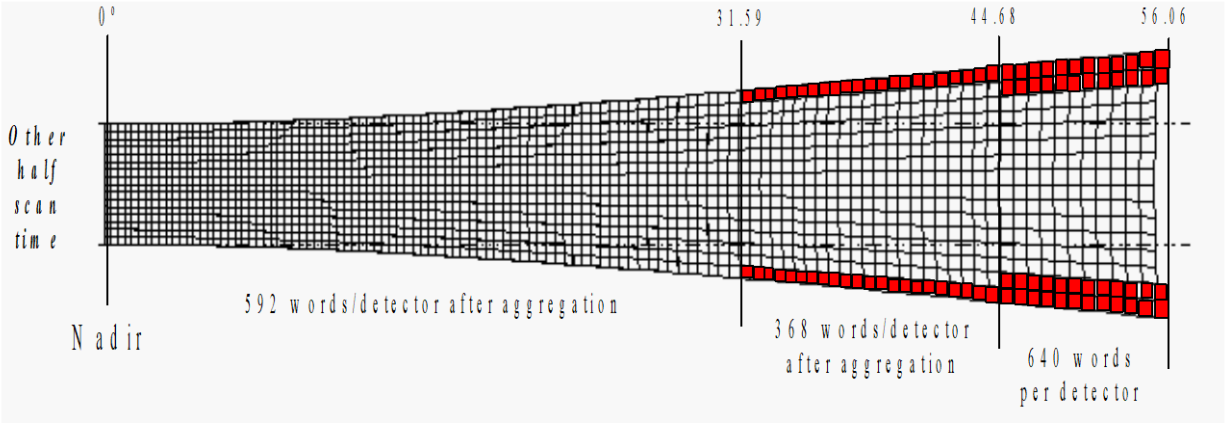

Figure 8. VIIRS aggregation and bowtie pixel reduction

The sensitivity performance of the VIIRS I-bands exceeds the Measurement Uncertainty threshold requirements by 30% or more.

3.2.5 VIIRS DNB Characteristics

The TOA radiance and TOA reflectance are produced over the entire operating range of the DNB. This results in potentially quantitative applications of DNB output ranging from full daytime to the new moon at night, but for the purposes of Imagery it allows for NCC Imagery EDR production over the same range of conditions. The SNR performance of the DNB at nadir is shown in Figure 9, while that for the edge-of-scan is shown in Figure 10.

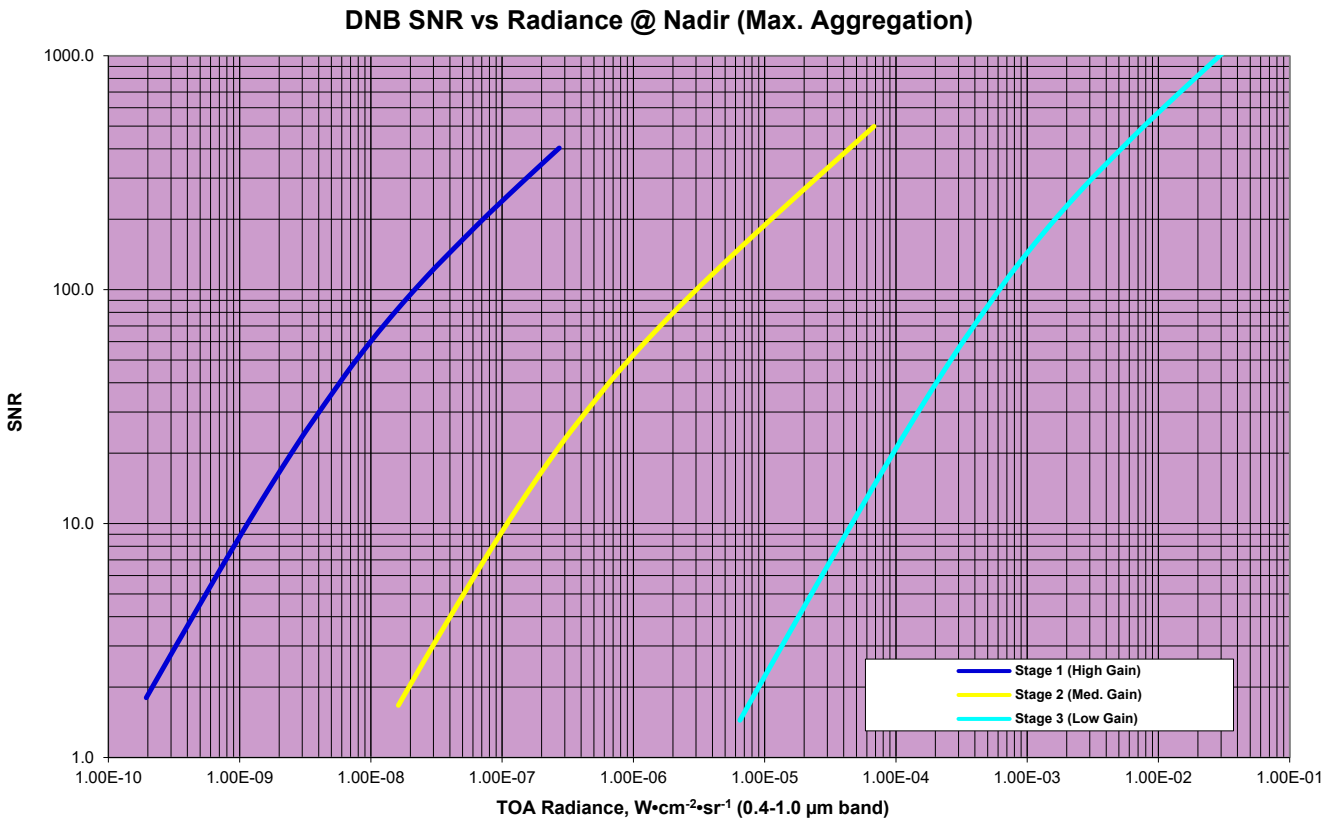

Figure 9. SNR performance for the DNB at nadir for each of the three CCD gain stages. SNR performance over the specified measurement range (4.0E-9 – 3.0E-2 W•cm-2•sr-1) is 30 to 1000. SNR greater than 3 is achieved at a radiance as low as 3.2E-10.

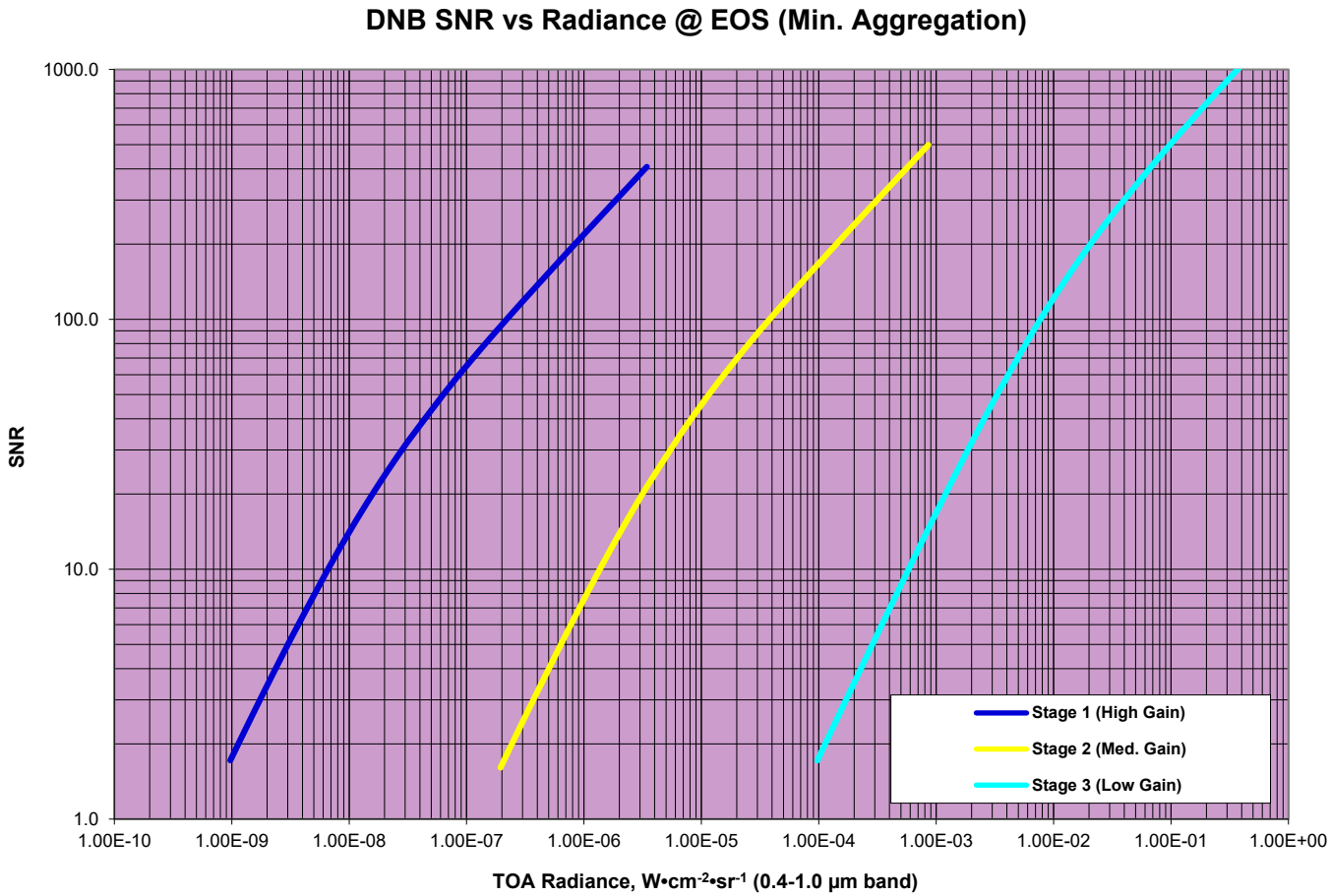

Figure 10. SNR performance for the DNB at edge-of-scan for each of the three CCD gain stages. SNR performance over the specified measurement range (4.0E-9 – 3.0E-2 W•cm-2•sr-1) is 7 to 250. SNR greater than 3 is achieved at a radiance as low as 1.8E-9.

The spectral response of the DNB was designed to operate efficiently under lunar illumination conditions, as shown in Figure 11.

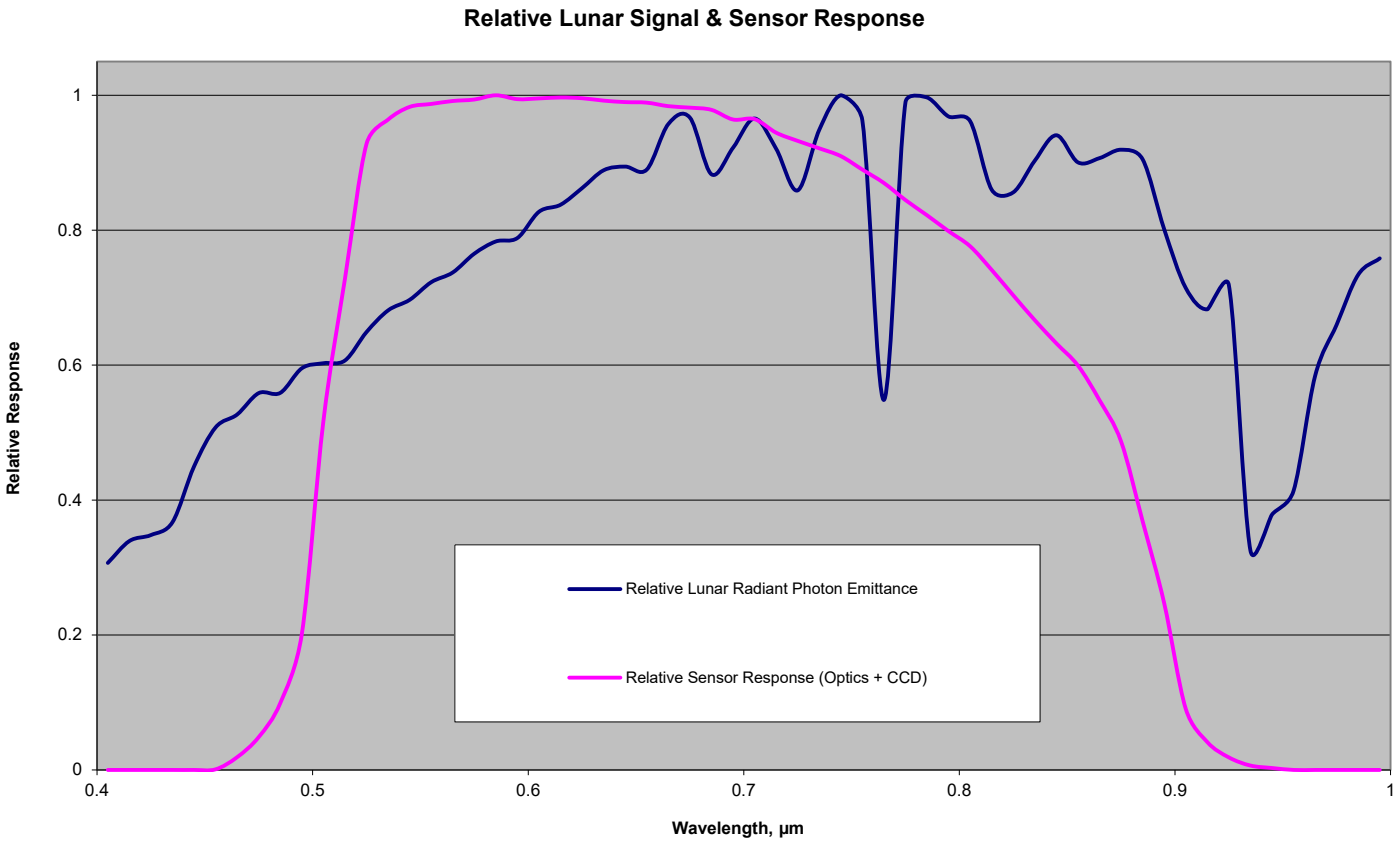

Figure 11. Spectral response of the DNB compared with the lunar signal

The spectral response of the DNB is designed to decline sharply at 0.5 µm, as can be seen in Figure 11. The purpose of the short-wave cut-off is to reduce contamination by atmospheric path radiance, which is more pronounced at shorter wavelengths. The design is compatible with OLS heritage.

DNB SDR performance at night varies with lunar phase, lunar elevation angle, and scan angle. An example for the quarter moon phase is shown in Figure 12.

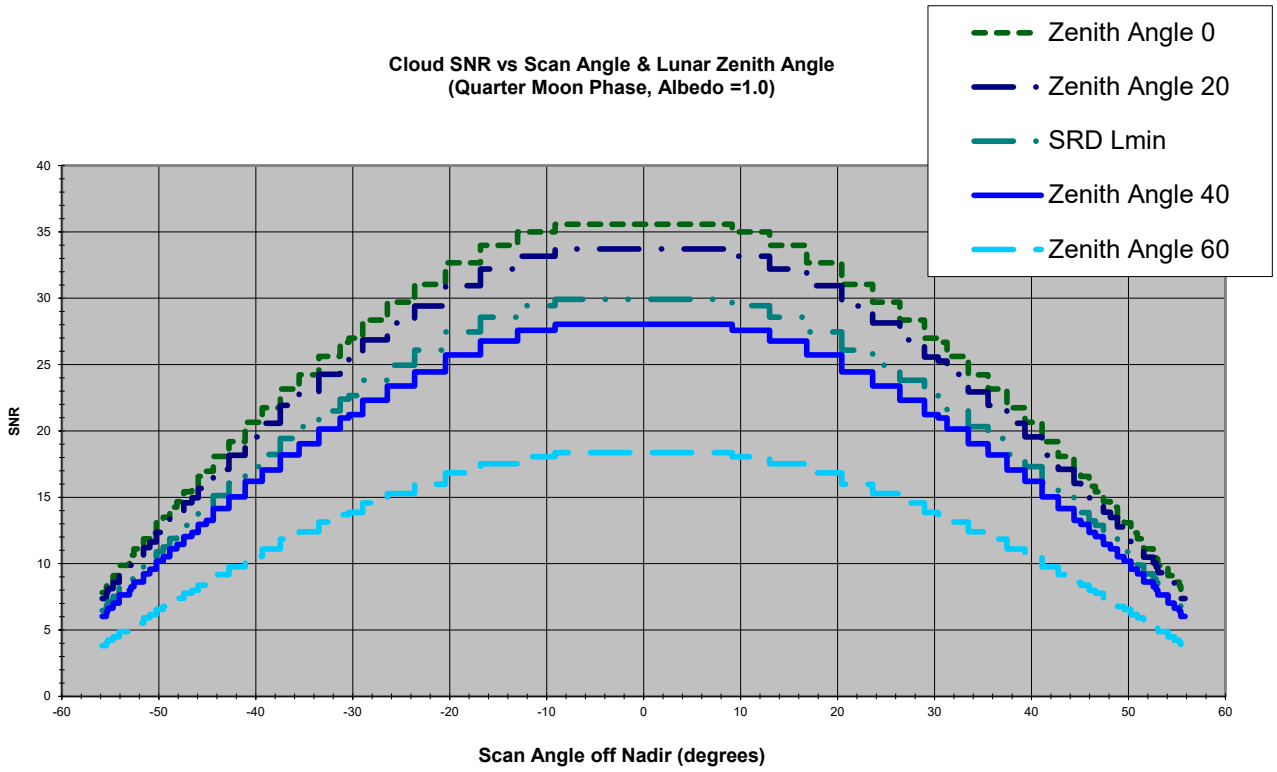

Figure 12. SNR performance of the DNB under quarter moon illumination conditions, as a function of scan angle.

The top two curves and bottom two curves represent lunar zenith angles of 0, 20, 40, and 60 degrees respectively. The middle curve corresponds to the minimum measurement range of 4.0E-9 $W \bullet cm^{-2} \bullet sr^{-1}$. SNR greater than 10 is achieved at the minimum radiance for almost the entire scan. SNR as high as 30 is achieved at the minimum radiance for a nadir view.

The sensitivity of the DNB has proven to be quite remarkable, and useful NCC Imagery is possible at night even when there is no lunar illumination. The presence of airglow has been shown to be sufficient for a potentially useful image to be created at night. Imagery users may need enhancement tools to bring out the contrast but unlike the older OLS, which is of little to no use once the lunar illumination is below the equivalent of the half-moon phase, NCC appears to be useful even when no moon is present.

3.3 NCC Imagery Production

3.3.1 Processing Outline

This section describes the NCC Imagery EDR ground processing algorithm. The NCC algorithm takes calibrated and geolocated DNB radiance as its input. Thus, before the algorithm can be executed, the RDR-to-SDR conversion of the DNB must have already occurred.

3.3.1.1 Baseline approach – GMA

The baseline approach adopted the same methods applied to the OLS processing algorithm for terminator imagery. This method was chosen to retain heritage with the DMSP mission.

The OLS terminator Imagery is produced via a GMA. The fundamental algorithm has been in use since the early 1980s. It is implemented by the OLS on-board Analog Signal Processor (ASP). The function of the GMA is to adjust the on-board analog gain to compensate for the variable source signal radiance. The Variable Digital Gain Amplifier (VDGA) operates in the ASP. A detailed description of the process can be found in the OLS Technical Operating Report (Westinghouse, 1993). Summarizing from the report:

"During active scan, the Along Scan Gain Control (ASGC) software controls the gain value presented to the VDGA. The computations performed for this control depend upon the spacecraft elevation, azimuth, and altitude, and the OLS scan angle. This computation produces the scene source elevation angle used to obtain a gain value from the Gain Value Versus Scene Source Elevation (GVVSSE) table. Thus, the software will cause the VDGA gain to follow the GVVSSE curve as defined by the GVVSSE table values."

Figure 13, created from data in the OLS Technical Operating Report; illustrates a typical GVVSSE (pronounced "Goosey") curve.

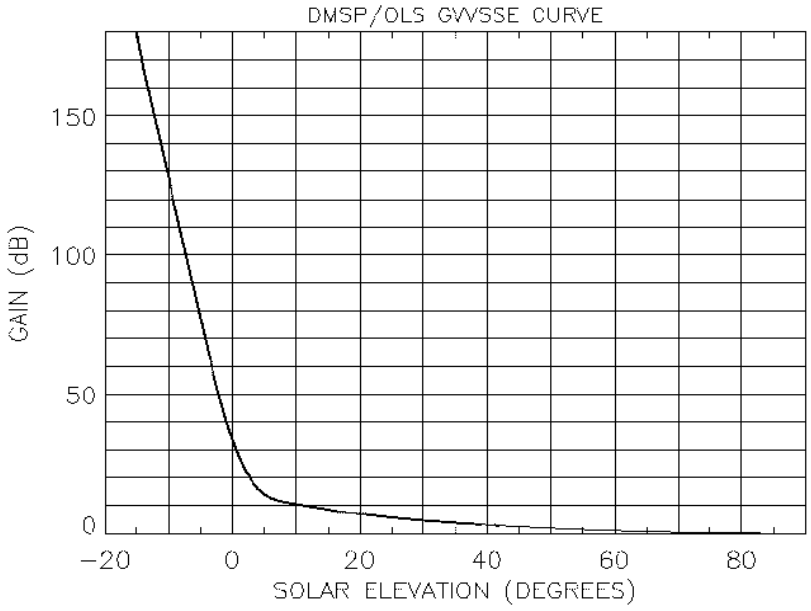

Figure 13. Typical GVVSSE curve for OLS on board variable gain control. The curve is designed so that a source with an albedo = 0.8 produces a 5 volt output signal from the analog signal processor. (Reference: OLS Technical Operating Report, March 1993)

Bi-directional Reflectance Distribution Function (BRDF) corrections are applied as adjustments of the elevation angle in the GVVSSE table. There is a comparable table, the Gain Value Versus Scene Lunar Elevation (GVVSLE), for a lunar source signal. Lunar BRDF and lunar phase corrections are also applied as adjustments of the elevation angle in the GVVSLE table. The function of the GMA is to adjust the OLS ASP gain so that a signal from a reflecting surface (cloud or ground) with an albedo of 0.8 and the modeled BRDF produces a 5 volt output signal from the ASP. The GMA was designed to accommodate the capabilities of late 1970s processors, and is implemented on board the OLS. The implementation of the VIIRS NCC algorithm occurs on the ground, within the IDPS. This approach provides the flexibility to make algorithm and LUT modifications easily via ground software changes, and takes advantage of the superior computational capability of the IDPS. This approach preserves the OLS heritage method by using LUTs that capture the gain and BRDF corrections applied on board the OLS.

The VIIRS implementation of the GMA algorithm operates as follows:

1) Read in the four pre-constructed LUTs into memory. These are the GVVSSE LUT, the Solar BRDF LUT, the GVVSLE LUT, and the Lunar BRDF LUT. Detailed descriptions of these LUTs may be found in the Data Dictionary for the VIIRS Imagery (2015).
2) Obtain DNB TOA radiance values from VIIRS DNB SDR. The TOA radiance is stored as a 2-dimensional array corresponding to each DNB pixel.
3) Obtain the latitude/longitude, solar, lunar, and satellite viewing angles, and lunar phase from the DNB SDR and associated geolocation file.
4) For pixels where the solar source radiance is sufficient (determined by the solar zenith angle, currently 105 degrees), compute the solar source radiance, using information in the GVVSSE and solar BRDF LUTs.
5) For all pixels, determine the lunar source radiance, using information in the GVVSLE and lunar BRDF LUTs. This step includes new moon conditions when there is no incoming radiance from either the sun or the moon, so NCC Imagery may be produced under virtually all conditions.
6) Convert the observed DNB TOA radiance for each pixel to a pseudo-albedo using the solar and lunar source radiances.
7) Write the pseudo-albedos to the Imagery EDR file, along with any associated quality flags.

The process flow for the NCC algorithm is illustrated in Figure 14. This process flow operates on each DNB pixel.

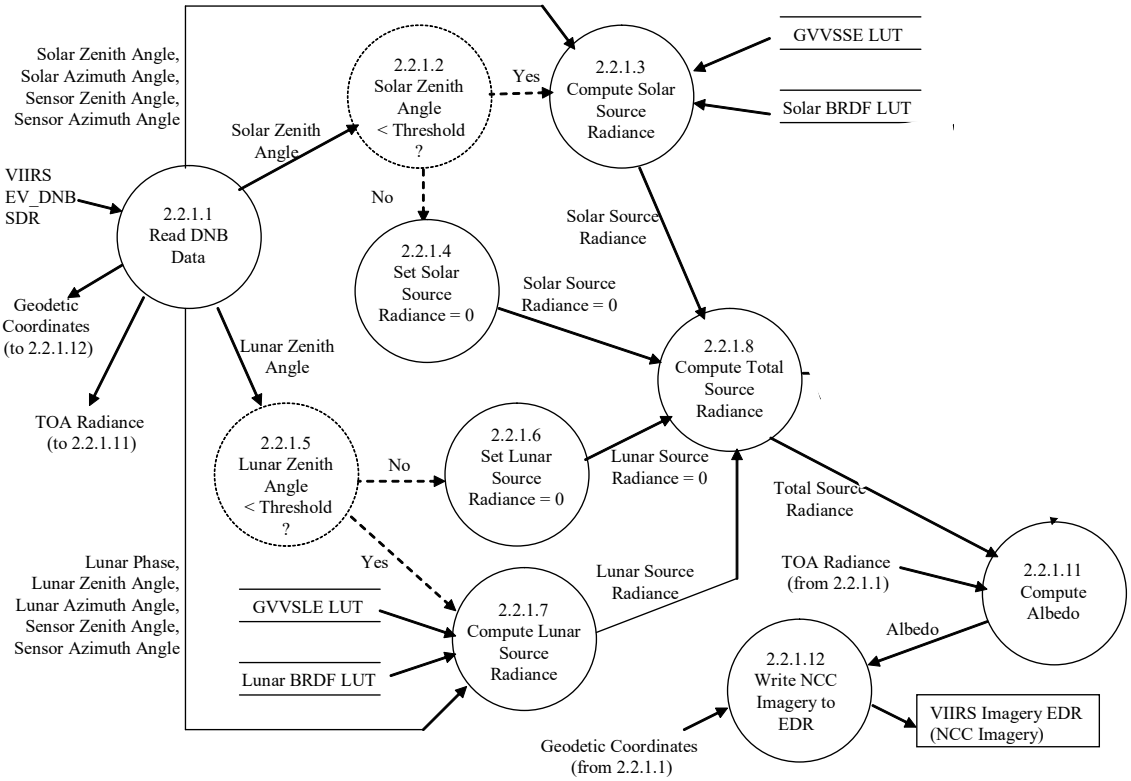

Figure 14. Process flow for the NCC Imagery algorithm

3.3.2 Algorithm Input

3.3.2.1 VIIRS data required for NCC Imagery

The NCC algorithm requires only the calibrated and geolocated data from the DNB SDR. These are supplied by the VIIRS DNB SDR.

3.3.2.2 Non VIIRS data required for NCC Imagery

The NCC algorithm requires four LUTs, described in the Data Dictionary for the VIIRS Imagery (2015). The GVVSSE LUT contains a solar gain function for a range of solar zenith angles (c.f. Figure 13). The GVVSLE LUT will contain a lunar gain function for a range of lunar zenith angles, similar to the GVVSSE function. The Solar BRDF LUT and Lunar BRDF LUT contain BRDF correction factors, binned by zenith angle, viewing angle, and relative azimuth angle.

3.3.3 Theoretical Description

3.3.3.1 Physics of the Problem

For decades, merged images (or "photo-mosaics") were produced manually by "cut and paste" methods and by photo-manipulation. More recently, automated methods have been developed that compute the merged image. These methods typically create a new image on a line by line basis. Each line may take data from one image up to a given point; beyond that point, data comes from the second image. The region adjacent to the switchover point is called the "seam".

An unintended feature of photo-mosaicing is the presence of visual artifacts that result from inherent differences between the two images that compose the merged image. The visual artifacts not only introduce potential confusion for the human analyst but can mask features of interest in the original images such as cloud type indicators or ice edge features. If one simply lines up two photos of the same scene taken at different times of day from the same vantage point and then cuts through the pair and tapes the opposite segments from the separate images together, one will immediately notice several artifacts. For example, if the contrast in one image does not match the contrast in the second or one is uniformly darker than the other (histogram mismatch), the analyst will notice an apparent edge at the seam joining the two halves. This seam is difficult to ignore since the eye responds preferentially to long straight features (e.g., edges, day/night texture changes, etc.).

Generically, artifacts can result from a number of inter-image differences. Some of these are content-related e.g., due to images taken at different times; some are sensor related, e.g., differences in dynamic range; some are platform-related, e.g., mis-registration errors; and some result from a combination of content and platform e.g., uncorrected parallax errors. The algorithm must accomplish the seam-finding and image combination in such a way so as to minimize the introduction of artifacts and subsequently must minimize their visual impact.

A further occasion for artifacts occurs due to the special processing required for pixels lying within the solar terminator. For the purposes of this ATBD, we identify the terminator region as the zone that is neither astronomical night nor standard daytime, approximately a solar zenith angle range of 75 to 105 degrees. These pixels may be saturated in the high-gain CCD stage while not being fully illuminated in the low-gain stage. The choice of grayscale value for the image therefore must maintain available contrast without introducing confusing artifacts or false contrasts.

The NCC EDR does not correspond to a single consistent physical characteristic of the natural environment. The resultant data product is used to provide the analyst an image for visual interpretation. The product is derived from the DNB, which has a separate algorithmic production process that must conform to the system requirements. The requirements that pertain to the NCC EDR instead relate to its usability for manual interpretation.

The NCC EDR must adequately represent the surface and atmospheric (specifically, cloud) conditions across the terminator region to be analyzed without artifacts due to the significant radiance difference (which range on the order of 1.E06 to 1.E07).

Image quality in the terminator region is also degraded by atmospheric scattering. Because of the low sun angle, the radiation transmitted downward to a reflecting surface (cloud or ground) travels longer path lengths, thereby increasing the amount of path radiance relative to reflected radiance. This is undesirable, since the primary purpose of image analysis is to detect the reflecting sources. Excessive path radiance washes out the image. In principle, atmospheric correction can remove the path radiance, thereby recovering the contrast between various reflecting surfaces. In practice, current Radiative Transfer Models (RTMs) are not capable of achieving satisfactory path radiance removal in the terminator region. As these models improve and hardware capabilities support near real time processing, an additional RTM-based adjustment may be added in the future to NCC production.

One other atmospheric characteristic that impacts NCC is the so called "airglow" or "nightglow". This feature primarily arises due to solar excitation of molecules during that day that lead to emission of photons by these molecules at night. This emission of photons acts as an additional source of illumination that ranges between ~1e-9 to 1e-11 $W \bullet cm^{-2} \bullet sr^{-1}$.

3.3.3.2 Mathematical Description of the Algorithm

The general procedures of the NCC algorithm are given below. The focus is on the terminator region where both solar and lunar components must be considered. The process executes if only one of these exists, though outside of the terminator the net impact to the resulting pseudo-albedos is small.

a) In the terminator region, the radiance of the DNB is often the result from both solar and lunar illumination. Starting from the night side of the terminator and beyond, i.e. ~100 to 180 degrees in solar zenith angle, the "airglow" or "nightglow" phenomena acts like an additional source of illumination and has a magnitude that ranges between ~1e-9 to 1e-11 $W \bullet cm^{-2} \bullet sr^{-1}$. Other sources of radiance, such as city lights, are not considered here. The combined radiance can then be expressed as:

   $L = L_{sun} + L_{moon}$

   Here the airglow radiance is included in L_{sun}.

b) The radiance components can be decomposed to those from atmospheric path (p) and those from the target (t: surface or clouds):

   $L = L_{sun\_p} + L_{moon\_p} + L_{sun\_t} + L_{moon\_t}$

   The target radiances, L_{sun_t} and L_{moon_t} are the radiances on the ground or at the top of the clouds.

c) The path radiance reduction procedure is to remove the path radiance from the total radiance, i.e. subtract the total radiance by the path radiance. Mathematically the resultant radiance becomes:

$L' = L - (L_{sun\_p} + L_{moon\_p}) = L_{sun\_t} + L_{moon\_t}$

Note that for the current baseline the path radiances are set to zero.

d) The normalization procedure is to divide this new radiance by the reference radiance of a reference surface.

$L_{norm} = L'/Lref = (L_{sun\_t} + L_{moon\_t}) / (Lref_{sun\_t} + Lref_{moon\_t})$
Where:

$Lref_{sun\_t} = \rho_{sarf} \cdot E_{sun} / \pi / G_{sun}(\Theta_{sun})$

$Lref_{moon\_t} = \rho_{larf} \cdot E_{moon} / \pi / G_{moon}(\Theta_{moon})$

The solar BRDF LUT provides the solar Anisotropic Reflectance Factor (ARF), ρ_{sarf}, and the lunar BRDF LUT provides the lunar ARF, ρ_{larf}. The GVVSSE LUT provides the solar-gain function $G_{sun}(\Theta_{sun})$, including the airglow contribution for solar zenith angles greater than ~100 degrees, and the GVVSLE LUT provides the lunar-gain function $G_{moon}(\Theta_{moon})$.

The GVVSSE and GVVSLE LUTs for the OLS system are empirically based. The baseline approach for NCC is to continue to use empirically-based tables, since RTMs are not reliable for solar or lunar zenith angles near the terminator. Empirically-based LUTs will be used until such time as a dependable RTM becomes available.

The significant radiance difference across the terminator due to illumination irradiance difference is normalized in L_{norm} and the resultant image product presents a near constant contrast across the scene.

Atmospheric effects due to absorption and scattering by aerosols are included in the empirical solar and lunar-gain functions. Since these functions represent averaged aerosol conditions, they do not allow for Atmospheric Optical Thickness (AOT) dependent adjustments. A future enhancement, as indicated above, would require an accurate and fairly fast RTM that produces reasonable results in the terminator region. Once that exists, the path radiances (L_{sun_p} & L_{moon_p}) do not have to be assumed to be zero and the appropriate adjustment would be added to the NCC algorithm.

3.3.4 Archived NCC output

The NCC algorithm output is a visible image at a resolution matching the GTM layout of the M-band Imagery EDR. The description of GTM may be found in Section 3.4. NCC Imagery is stored as an Imagery HDF5 file with the associated quality flags.

3.3.5 Performance of NCC Imagery

The NCC algorithm is best revealed by using an example of the DNB SDR and the resulting NCC Imagery EDR in a terminator setting. In Figure 15the top image shows a DNB (SDR) granule that crosses the day/night terminator. The lower image shows the associated NCC (EDR) granule (with edge fill values highlighted in blue). The NCC process reduces the contrast from solar and lunar illumination gradients across the granule (which spans over 7 orders of magnitude between day and night) by converting it to a quantity with reduced dynamic range (i.e. pseudo-albedo). The result is an image with nearly constant contrast across the entire scene. By this process, nighttime images of clouds should, in principle, appear very similar to solar reflectance-based daytime imagery.

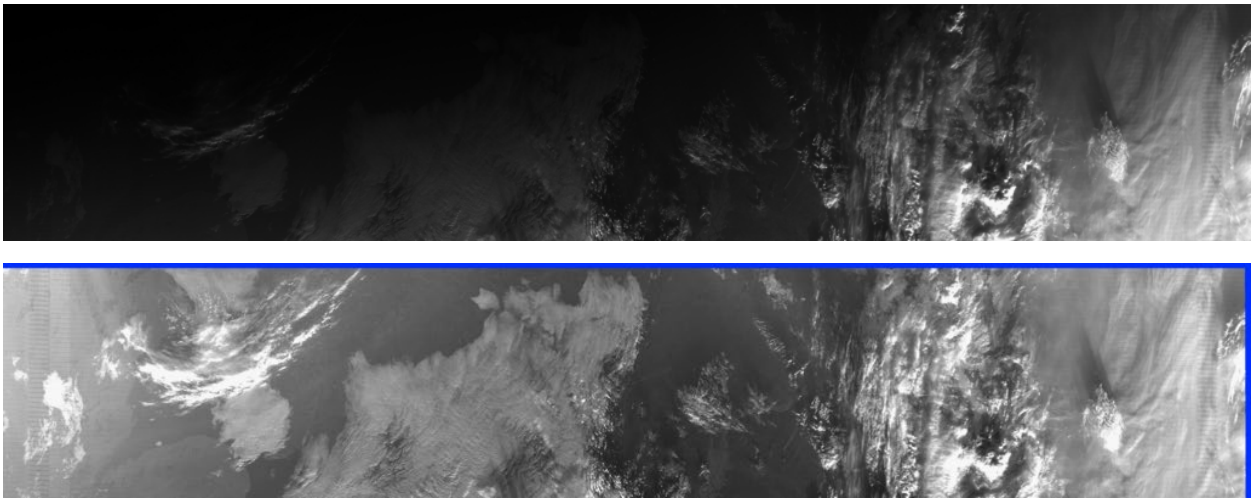

Figure 15. Example of DNB SDR (top) versus NCC Imagery EDR (bottom).

Artifacts in the DNB SDR will be inherited by the NCC Imagery EDR. Before August 2013 the most significant of these was a stray light issue with the DNB just on the dark side of the terminator. The DNB SDR algorithm was adjusted to correct for this error in August 2013. The impact on the NCC Imagery EDR was profound, and an example is shown in Figure 16. The removal of the stray light is evident in Figure 16, taken from the granule over the upper Midwest of the US on 9 August 2013. As a reference, Lake Michigan may be seen in the middle of the granule.

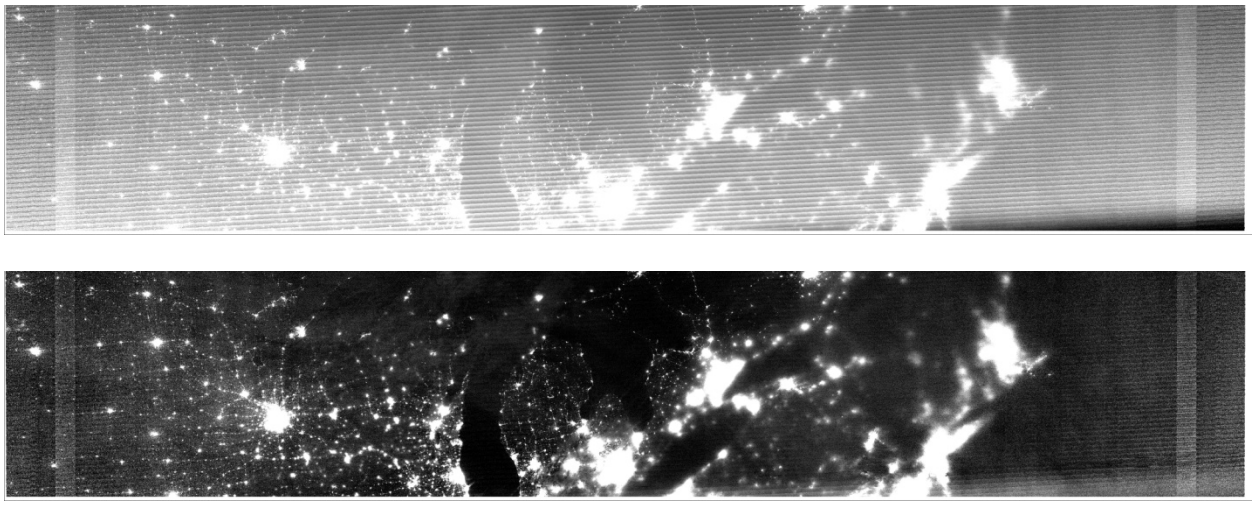

Figure 16. NCC Imagery taken over the US Upper Midwest on 9 August 2013. The top portion of the figure is how the NCC Imagery would appear without the stray light correction in the DNB SDR, the lower image is after the stray light correction is applied.

The NCC Imagery EDR is produced under all solar and lunar illumination conditions, including cases where there is no illumination from either the sun or moon (i.e. new moon phase). The DNB is sensitive enough that air glow is sufficient to create an image, although such an image appears quite noisy. Figure 17 contains an example of NCC Imagery at night when the moon was below the horizon. The example is Super Typhoon Phielin taken on the night of 10 October 2013. The typhoon, along with convective elements and its eye, are evident despite the extremely low levels of radiance present in the DNB spectrum. The bright rectangular shapes in the image are caused by lightning. This is, in essence, the "worst case" scenario for NCC Imagery. As lunar illumination increases, the SNR improves and the noisiness in the DNB SDR decreases, with subsequent benefits to the NCC Imagery EDR.

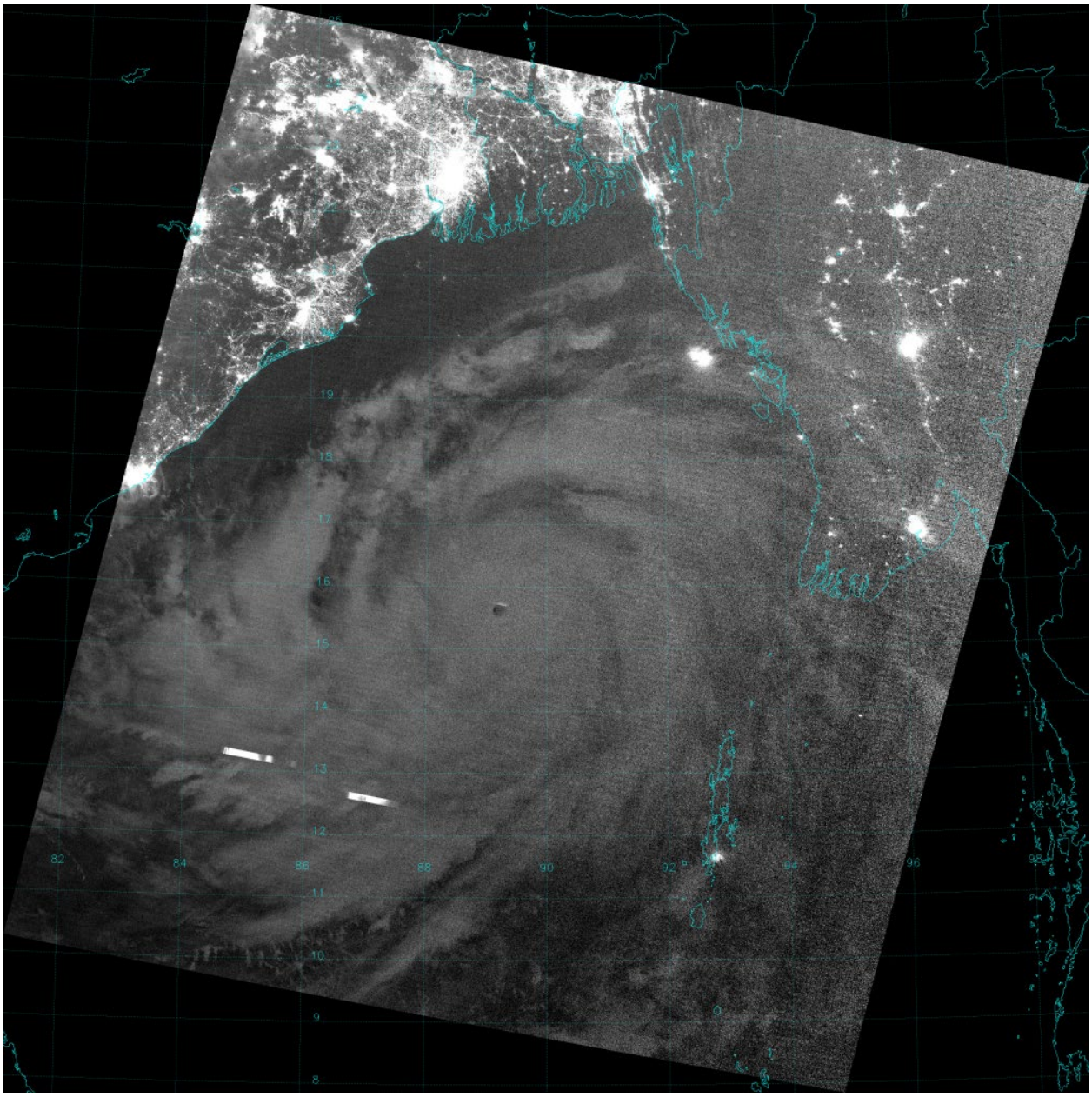

Figure 17. Example of NCC Imagery at night with no lunar illumination

With the removal of the stray light artifacts, and the capability to produce an image even under no illumination from either a solar or lunar source, NCC Imagery presents the user with a capability beyond known nighttime visual Imagery capabilities to date. Additional examples may be found in the Imagery EDR User's Guide (Seaman et al, 2015) and an article in the *Bulletin of the American Meteorological Society* by Hillger et al (2013).

The DNB output on NOAA-20 is not the same as that for SNPP. The DNB, and only the DNB, contains what is referred to as an "extended granule". (This extended granule is not expected for the DNB SDRs from JPSS-2.) A non-linearity issue was discovered that impacts the VIIRS DNB

on these two satellites, and the optimal solution was to create an asymmetric DNB SDR. This asymmetry means nadir is not in the center of the DNB SDR output, and the scan line is longer on one side of nadir versus the other. However, for GTM nadir must be in the center. Note this asymmetry only applies to the DNB and not any of the other bands on VIIRS.

The Imagery algorithm handles this by first building the GTM, then mapping the appropriate DNB pixels into the GTM. The result is the "extended" portion is cut off from the display. This is shown in Figure 18, which contains a DNB SDR output and the resulting NCC Image EDR. Note how the NCC image placed nadir in the center of the image, and the extended component is not present. This allows Imagery users to employ NCC as part of a multi-spectral image with any other GTM-based Imagery product without having to make any additional adjustments. Forcing the extended portion of the SDR into the GTM either distorts the image on the side of the extended portion or breaks the GTM paradigm of nadir being the center of the image.

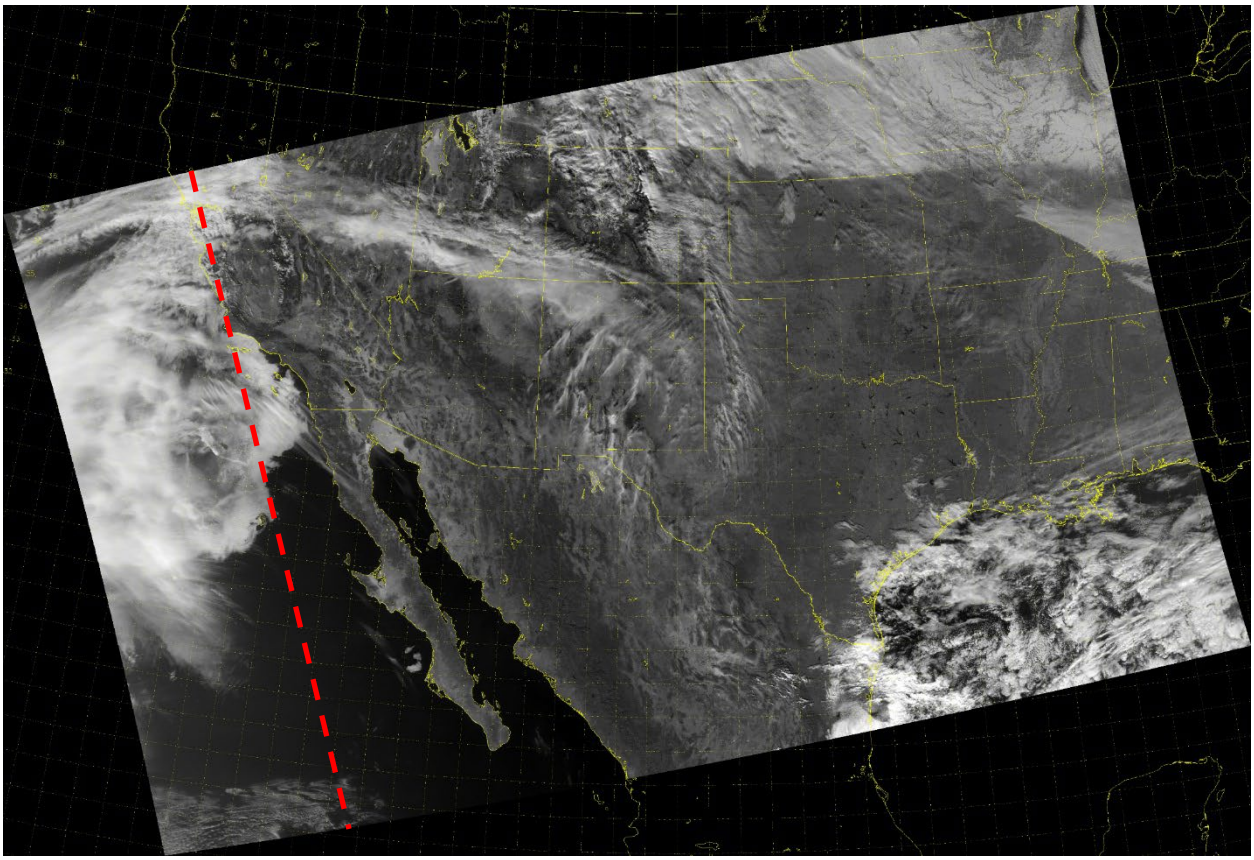

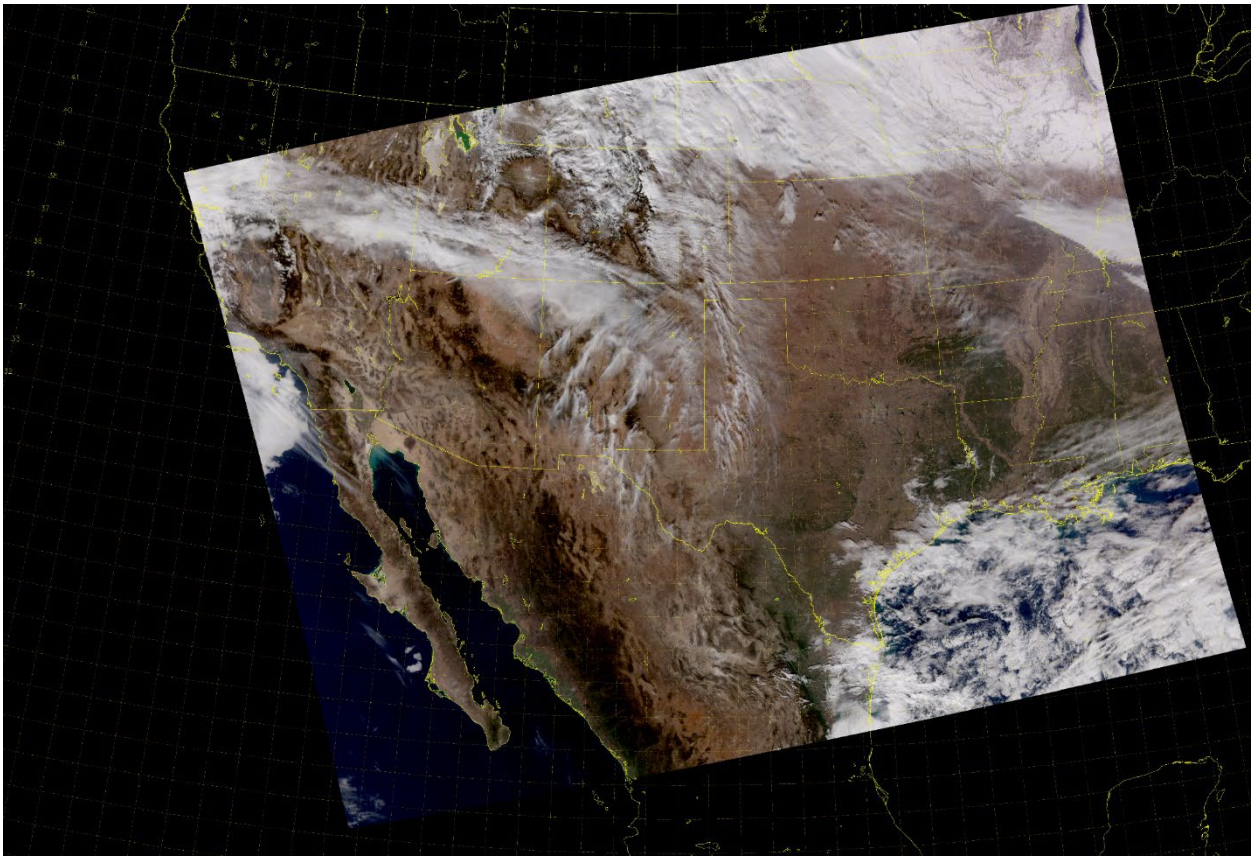

Figure 18. Example of DNB SDR and resulting NCC Imagery, data was taken from granules on 5 January 2018 over the Southwest US. The dashed red line indicates the portion of the SDR that comprises the extended portion of the DNB SDR.

3.3.6 Initialization and Validation

3.3.6.1 Initialization

The baseline algorithm is based on proven OLS heritage. The LUTs used by the algorithm are generated offline. The original LUTs were based on OLS gain and BRDF values to preserve continuity, but since the launch of Suomi National Polar Orbiting Partnership (S-NPP) LUTs specific to VIIRS SDR measurements are employed, while the principles of the original approach are maintained.

3.3.6.2 Pre-launch Characterization

Before the launch of S-NPP, the algorithm was developed and tested using OLS Imagery obtained from the National Geophysical Data Center (NGDC). The functionality of the NCC approach was validated at that time. Since the algorithm applies straightforward LUTs, the impact to latency was quickly shown to be minimal.

3.3.6.3 Validation

NCC Imagery was one of the first products produced after the activation of VIIRS. Since the purpose of the algorithm was to reduce/minimize solar/lunar illumination gradients across the scan, validation was done primarily through visual inspection of the NCC Imagery EDR. Daytime and terminator scenes, such as the one in Figure 15, indicated early in the program that the NCC process fundamentally worked. The one error exclusive to the NCC algorithm was the creation of fill pixels when the (lunar) illumination was quite small. When this occurred, the NCC Imagery was not useful. The issue was traced to the limits set of the computation and allowed values of the pseudo-albedo. Once this was corrected, the NCC product performed as expected.

3.3.7 Practical Considerations

3.3.7.1 Numerical Computation Considerations

The baseline algorithm was already operational on the DMSP and poses no numerical computation problems. The solar and lunar-gain values are obtained from direct interpolation of 1-d LUT arrays, with no inversion, iteration, or search window functions. The BRDF values are also obtained from direct interpolation of LUT arrays. Though these are multidimensional, their size is small enough to allow rapid processing.

3.3.7.2 Programming and Procedural Considerations

All the NCC Imagery EDR procedures are automatic to perform in an operational environment. If one or more of the LUTs requires an update, the update is performed offline. LUT updates are quite infrequent, no more than once per year.

3.3.7.3 Configuration of Retrievals

The NCC algorithm requires the VIIRS DNB SDR and four VIIRS LUTs as input. The output of this algorithm is for analyst manual interpretation and does not serve as quantitative input to any other EDRs. The IDPS processing configuration is designed to satisfy these expectations.

3.3.7.4 Quality Assessment and Diagnostics

In general, the NCC image should resemble the DNB input, as modified by the NCC process. If these products are insufficient to support manual analysis, then the NCC product is unlikely to serve the analyst, though this depends fundamentally on the quality of the DNB SDR. Thus, if there is little moonlight, contrast is generally poor (e.g. Figure 17) however, it is usually sufficient to identify clouds. Sun glint also impairs manual analysis. The algorithm software is designed to set NCC quality flags for each DNB pixel. The flags are set if there is a processing problem with the solar gain, solar BRDF, lunar gain, lunar BRDF, and/or path radiance derivations. If either the observed DNB TOA radiance or the computed source radiance for a given pixel is less than a minimum threshold (currently set as the measurement range minimum of 4.0E-9 $W \bullet cm^{-2} \bullet sr^{-1}$), a low radiance quality flag will be set for that pixel. However, a NCC Imagery EDR is still produced.

3.4 Ground-Track Mercator (GTM) Imagery Product Description

The purpose of the VIIRS GTM Imagery algorithm is to map VIIRS Imagery (I) band data, Moderate (M-band) data, and pseudo-albedo values from the NCC algorithm onto GTM coordinates. The GTM layout is a grid of pixels, where rows are at right angles to the ground track and columns are parallel to the ground track. This GTM layout does not have the "bow-tie" effect. The GTM Imagery EDR products are primarily used for human viewing, specifically for atmospheric and ground features such as clouds and sea ice.

The GTM is not a map projection, i.e., it does not have an exact set of unchanging transformation equations. Rather, a numerical integration process allows a latitude/longitude calculation of a row/column (X, Y) position on the map plane, or vice versa. The actual ground track (nadir) of the spacecraft establishes the map plane; consequently, the map plane is different for every orbit. The GTM map has an advantage of always having the ground track (nadir) in the center of the map plane. Furthermore, multiple granules of satellite data can be concatenated without having to switch from one orbit path map to another.

JPSS creates two kinds of GTM maps: Fine and Coarse. The Fine GTM map has a pixel center spacing of 375 m, which is close to the nadir sample distance of the VIIRS Imagery resolution (I) bands. The Coarse GTM map has a pixel-center spacing of 750 m, which is close to the nadir sample distance of the VIIRS Moderate resolution (M) bands. The pixel spacing in the along-track direction is equal to the pixel spacing in the cross-track direction. The maximum variation, in both conformality and area per pixel, is about one percent. The X-coordinate on the GTM map increases in the direction of spacecraft motion along the ground track. The X axis is precisely on the ground track, and is derived from the spacecraft diary. The Y axis of the map is at a right angle to the X axis. That is, the rows of the GTM map are always at an exact right angle to the ground track. The time attached to each row of the map is the time the spacecraft passes over the nadir point of that row. Figure 19 shows how this configuration works.

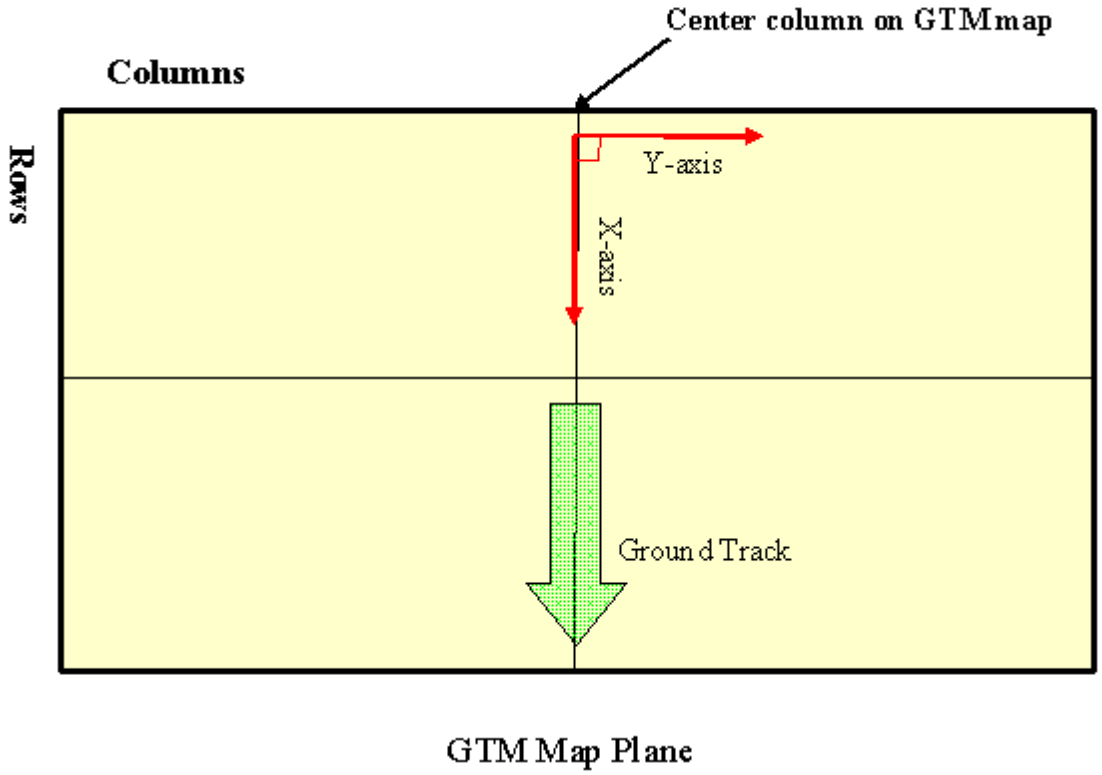

Figure 19. GTM Map Attributes

A 3090 km GTM swath was chosen to accommodate a maximum satellite altitude of 850 km. There are 1541 rows and 8241 columns in the fine resolution GTM layout, with 771 rows and 4121 columns in the coarse GTM layout. The row size was chosen to accommodate the minimum altitude (maximum distance of a granule) of the satellite. There can be a variable number of empty columns on the edges of the swath, due to a larger area of the Earth's surface seen near the poles and less near the equator. Rows pull together slightly at the swath edges due to Earth curvature and horizontal size of the GTM swath. There are also a variable number of empty rows at the bottom of the GTM rectangle, due to the fixed horizontal sample distance and forward ground motion of the spacecraft. This layout allows concatenation of an unlimited number of EDR granules without any discontinuities, even at the poles. Because the delivered Imagery product retains a constant array size, the empty rows and columns are evident at the edges of an Imagery granule, and it is left to the user to remove them if they wish.

The center column of the coarse map exactly follows the center column of the fine map. The pixel centers of the coarse map center column are the same as every other pixel of the fine map center column. Similarly, the pixel centers to the left and right of the center column on the coarse map have the same centers as every other pixel on the corresponding row of the fine map. Therefore the scaling from the coarse map to the fine map is always an exact factor of two. Once the locations of the fine GTM map are established, the locations of the coarse GTM map are determined by a simple 2x2 decimation. In Figure 20 each dot represents a pixel center on the GTM fine map. The emphasized dots represent coarse pixels on the fine map.

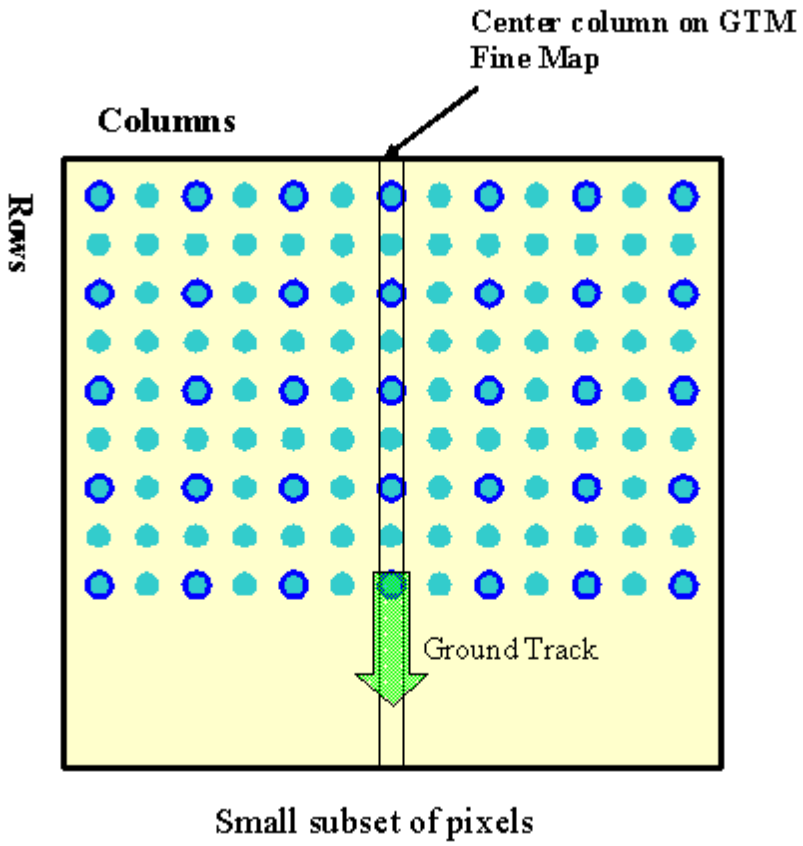

Figure 20. Fine map pixels with emphasized coarse pixels.

Even though the characteristics of the VIIRS sensor have been used to establish the parameters of the GTM maps, any kind of data can be remapped to the GTM maps. This makes it possible to form matching overlays from any number of data sources.

3.4.1 Processing Outline

The first step in creating the GTM map data for a VIIRS granule is to obtain the ground track from the VIIRS SDR geolocation software and the spacecraft diary. The geolocation function provides the geodetic latitude, longitude, and direction of ground track motion, at least once per second. The basis of this ground track data is the ephemeris data reported by the Global Positioning System (GPS) sensor on the spacecraft. This data comes down in the Ephemeris and Attitude data packets (these packets are also called "spacecraft diary" packets). Notice the direction of ground track motion is in the Earth Centered Rotational (ECR) system of the rotating Earth. This means the direction of ground track motion accounts for the rotation of the Earth as well as the inertial motion of the spacecraft.

Once the locations of the ground track column pixels are established, it is possible to calculate the locations of the pixels along the rows by a simple application of spherical trigonometry. The geodetic latitude and longitude of the center pixel are used along with the radius of the Earth at that geodetic latitude. The direction from the center pixel to another pixel in the row is exactly 90

degrees to the left or right of the direction of ground track motion, which means the row is at an exact right angle to the ground track. All the pixels in one row of the map are theoretically at the same time as the center pixel, so there is no spacecraft motion or Earth rotation to account for along each row. The fact that the Earth is not an exact sphere is not a problem, since the objective is a reproducible map where there is a "one-to-one and onto" relationship between the surface of the Earth and the GTM map. In summary, great circle distance and spherical trigonometry, the location of the pixel in the center of each row, and direction of ground track motion are used to establish the location of each pixel along the row.

3.4.2 Algorithm Input

The GTM algorithm uses a relatively small, single set of data: 1) the ephemeris data recorded by the GPS sensor on the spacecraft during the time span of the granule, 2) the deterministic granule boundaries (start and stop time of each granule) of the spacecraft, and 3) the 375 m Earth surface distance between each pixel of the Fine GTM map. VIIRS I-band Imagery algorithm requires several types of data to perform mapping to the GTM layout, summarized in Table 3. Recall the coarse layout is based on that from the fine scale layout.

Table 3. VIIRS I-band Imagery EDR inputs

Name	Description
Spacecraft Diary RDRs	Altitude and ephemeris data for the granule
VIIRS I1, I2, and I3 SDRs	Radiances and reflectances along with granule boundary times and granule mode. Used for day and mixed mode granules.
VIIRS I4 and I5 SDRs	Radiances and brightness temperatures along with granule boundary times and granule mode. Used for day, mixed, and night granules.
VIIRS I-band Geolocation	Geolocation data for every pixel in the granule.
VIIRS I-band gridded geolocation	Map grid row and column values for every pixel in the granule
Bands I1 – I5 Data Quality Threshold Tables	An optional input used for performing quality checks on the data.

3.4.3 Theoretical Description

The common geolocation process is used to calculate the ground track points for the start time and end time of the granule. Then a combination of spherical trigonometry and common geolocation functions are used to space the rows of the fine GTM map as close to 375 m as possible, and to put the center of the map precisely on the ground track. For the present granule size of about 85.752 s, there are approximately 1536 rows for Image (I-band) resolution and 768 rows for Moderate (M-band) resolution of actual data. The number of rows varies slightly because the

granule size is a fixed number of seconds, and the ground track speed of the spacecraft varies slightly, but it is important to remember the final size of the output array is constant (see Section 3.4). The maximum variation in row spacing at nadir is 375 m, +/- about 0.7 m. Careful location of the first and last row in one granule means the GTM map of one granule always precisely concatenates with the GTM maps of the neighboring granules. Thus, the centers of each row of the GTM map, the ground track pixels, are located by equal distance spacing of the pixels precisely on the ground track.

The operational software only does full calculations for every 10^{th} row and column, and then does quadratic interpolation of the pixels between. This ensures the calculation of a full set of latitudes and longitudes for a map is a relatively fast process.

The process of converting row and column to latitude and longitude, and vice versa, can be done by two methods. Method 1 is based on the fast search of a full set of geolocation data for the GTM map. Method 2 works from only the ground track data and works by an iterative search of the ground track, followed by a spherical trigonometry calculation along the row. Method 2 is slightly faster and the difference between the results is always less than 1 m (the size of floating point round-off to 32 bits). The Nearest Neighbor method is used for filling pixels to preserve contrast and sharpness for human viewing. If full geolocation accuracy of the Sensor Data Record (SDR) is needed, the SDR should be used and not the GTM Imagery EDR. Since it is slightly faster, the Imagery EDR uses Method 2.

Based on mode (day, mixed, or night) of the granule, data from either two or five I-bands are mapped onto the GTM map. In other words, two or five separate EDRs are created along with geolocation data for a given granule. Radiance and reflectance values for bands I1 through I3, along with radiance and brightness temperature values for bands I4 and I5, are processed for "day" and "mixed" mode granules. Radiance and brightness temperature values for bands I4 and I5 are processed for "night" mode granules. M-band Imagery EDRs are created using the short names VIIRS-M1ST-IMG-EDR through VIIRS-M16TH-IMG-EDR. The DNB is processed by the NCC Imagery algorithm to produce an EDR mapped to GTM.

3.4.4 Archived GTM Imagery output

VIIRS I-band Imagery EDRs are summarized in Tables Table 4-Table 5. Note the first three I-bands have a reflectance field while I4 and I5 EDRs contain a brightness temperature field. The VIIRS I-band geolocation or GEO file is summarized in Table 6. Details of the entire file may be found in the Data Dictionary for the VIIRS Imagery (2015).

Table 4. VIIRS I-band Imagery EDR Output

Output	Type	Description
Radiance	Uint16 * [1541 * 8241]	TOA radiances for bands I1 – I5

Reflectance	Uint16 * [1541 * 8241]	TOA reflectances (daytime only) for bands I1 – I3
Brightness Temperature	Uint16 * [1541 * 8241]	TOA EBBT for bands I4/I5
Pixel quality	Uint16 * [1541 * 8241]	Pixel level quality flags
radScale	Float 32	Scale for scaled radiances
radOff	Float 32	Offset for scaled radiances
refl/btScale	Float 32	Scale for Reflectance/Brightness Temperature
refl/btOff	Float 32	Offset for Reflectance/Brightness Temperature

Table 5. VIIRS I-band Imagery EDR Pixel Level Quality Flags

Bits	Description	Values
0-1	Imagery Quality (Pixel Quality as determined by the SDR Calibration Quality). Note that individual bad pixels in the Imagery EDR are filled by an average of the two adjacent pixels. If the bad pixel is edge-of-scan, the Imagery EDR uses the adjacent pixel.	0: Good 1: Poor 2: No Calibration 3: Dead pixel replacement
2	Pixel is saturated	0: False 1: True
3-4	Missing Data (Data required for calibration processing is not available)	0: All data present 1: Earth View missing 2: Cal data missing 3: Therm data missing
5-6	Out of Range	0: Good 1: Radiance out of range 2: Reflectance out of range 3: Both out of range
7	Spare	

Table 6. VIIRS I-band Imagery Geolocation (GEO) Outputs

Output	Type	Description	Units/Range
rowTime	Int64 * [1541]	Time of the nadir point of the GTM row in IDPS Epoch Time (IET – 1/1/1958).	Microseconds/ 1483228832000000 to 2272147232000000
Latitude	Float32 * [1541 * 8241]	Latitude of each pixel (positive North)	Degrees/ -90 to 90
Longitude	Float32 * [1541 * 8241]	Longitude of each pixel (positive East)	Degrees/ -180 to 180

sunZenith	Float32 * [1541 * 8241]	Zenith angle of the sun at each pixel position	Degrees/ 0 to 180
sunAzimuth	Float32 * [1541 * 8241]	Azimuth angle of the sun (measured clockwise from North) at each pixel position	Degrees/ -180 to 180
sensorZenith	Float32 * [1541 * 8241]	Zenith angle of the satellite at each pixel position	Degrees/ 0 to 180
sensorAzimuth	Float32 * [1541 * 8241]	Azimuth angle (measured clockwise positive from North) to satellite at each pixel position	Degrees/ -180 to 180
terrainHeight	Int16 * [1541 * 8241]	Ellipsoid-Geoid separation	Meters/ -500 to 8300
satRange	Float32 * [1541 * 8241]	Line of sight distance from the ellipsoid intersection to the satellite	Meters/ 820,000 to 1,900,000
pixelQuality	Uint8 * [1541 * 8241]	Pixel level geolocation quality flags	See Table 7
scanQuality	Uint8 * [48]	Scan level geolocation quality flags	See Table 8
sdrRow	Uint16 * [1541 * 8241]	Imagery SDR pixel row index number	Unitless
sdrCol	Uint16 * [1541 * 8241]	Imagery SDR pixel column index number	Unitless

Table 7. VIIRS I-band Imagery GEO Pixel Level Quality Flags

Bits	Description	Value
0-1	SDR Pixel Mapping Coordinate (GTM to SDR). Indicates whether this pixel originated from the previous, current, or next granule in the SDR Imagery Resolution (I-band) Geolocation	0: Error 1: Previous Granule 2: Current Granule 3: Next Granule
2-7	Spare	

Table 8. VIIRS I-band Imagery GEO Scan Level Quality Flags

Bits	Description	Value
0-1	Solar Eclipse	0: No Solar Eclipse 1: Solar Eclipse
2-7	Spare	

M-band Imagery EDRs follow the same structure as the I-bands, but with half the array size (771 by 4121). The geolocation parameters are the same as those for the I-bands. Details of the M-band Imagery EDR formats are also found in the Data Dictionary for the VIIRS Imagery (2015); recall the M-band Imagery EDRs are not archived. The NCC EDR follows the M-band paradigm, but instead of radiance and reflectance only reports a pseudo-albedo that is unitless. The NCC EDR geolocation includes three additional parameters concerning lunar geometry. These are shown in Table 9.

Table 9. Additional parameters contained with the NCC geolocation file

Output	Type	Description	Units/Range
MoonIllumFraction	Float32	Fraction of the moon illuminated	Unitless
LunarZenithAngle	Float32 * [771 * 4121]	Zenith angle of the moon at each pixel position	Degrees/ 0 to 180
LunarAzimuthAngle	Float32 * [1541 * 8241]	Azimuth angle of the moon at each pixel position	Degrees/ -180 to 180

3.4.5 Practical Considerations

3.4.5.1 Graceful Degradation

Graceful degradation is only noted in the Imagery Geolocation file. If an input (SDR) retrieved for the Imagery algorithm has its "N_Graceful_Degradation" metadata field set to YES (propagation), then the appropriate quality flag will indicate degradation for Imagery.

3.4.5.2 Exception Handling

Missing sensor data caused by bad detectors are replaced during the creation of the Imagery as follows: For edge of scan, the radiance value of the adjacent pixel is copied into the missing pixel. For non-edge of scan, the radiances are averaged using the two adjacent pixels and copied into the missing pixel. The GTM algorithm is capable of handling an entire scan line identified as "bad" (if identified by FILL values) and will search the adjacent pixels perpendicular to the bad pixels, replacing FILL with an average radiance/reflectance/EBBT. If a bad pixel is not properly flagged, it will appear in the Imagery product and interfere with the visual use of that image. The I3 SDR on NOAA-20 has such "bad" scan lines due to a bad detector, but the Imagery algorithm successfully removes the effects from the image. Should striping from bad pixels exist in any SDR, the Imagery algorithm removes them from the resulting product. Other causes of striping are not removed. Additionally, the VIIRS GTM Imagery software is designed to handle a wide variety of processing problems. If the granule contains the necessary SDRs and geolocation, an Imagery EDR will always be created.

3.4.5.3 Numerical Computation Considerations

The original NPOESS requirements included a specific paragraph stating the Imagery EDR must be produced from the RDRs in 20 minutes or less. The IDPS easily meets this requirement; the actual time taken to go from RDRs to Imagery is less than 10 minutes on the operational system. The GTM process is not computationally expensive. NCC processing is accelerated by the use of pre-existing LUTs. All processes for creating Imagery are automatic. There are no concerns with the development and creation of Imagery EDRs with the IDPS algorithm or its related processing software on Field Terminals.

3.5 Terrain Correction

Users tracking fires at night through the DNB noticed that it appeared these fires moved or shifted when comparing Imagery results covering the same area. When city lights were observed to do the same thing, it was recognized this was a false signature based on Imagery using the Ellipsoid instead of compensating for terrain heights. In 2018 the JPSS program updated the Imagery requirements to replace the Ellipsoid with Terrain Corrected Imagery. This prevents the apparent shifting that occurs between different passes observing the same feature.

Initial expectations that the software would accommodate a simple change from using the Ellipsoid to the Terrain Corrected geolocation proved incorrect. The actual geolocations used by the Imagery software were from an intermediate and temporary file created by the geolocation software, one that only produced such an intermediate file for the M-bands. A team of Geolocation and Imagery team members worked through this conundrum and successfully created, and then read in, these new files for all band types (I-band, M-band, and DNB). Each of these internal files are retained in memory only as long as needed for the Imagery products to be produced. Only one internal file is needed for each Imagery type. Impacts of these updates are shown in Figure 21.

The example below is taken from a granule on 15 May 2018, where the Rocky Mountains lie to the east of nadir, while the Pacific Ocean lies to the west. With Terrain Correction applied, features over or containing high terrain, but away from nadir, will shift towards nadir relative to an Image on the Ellipsoid. Given the size of this shift is small when looking at an entire granule, arrows are used to show the variation in the shift. The portion of the image shown covers the Rocky Mountains over Colorado and southern Wyoming. The maximum shift in this figure is approximately 8 I-band pixels (or about 3 km) but the shift will vary based on the actual terrain height and the distance of the pixel from nadir. The arrows in Figure 21 are not drawn to scale.

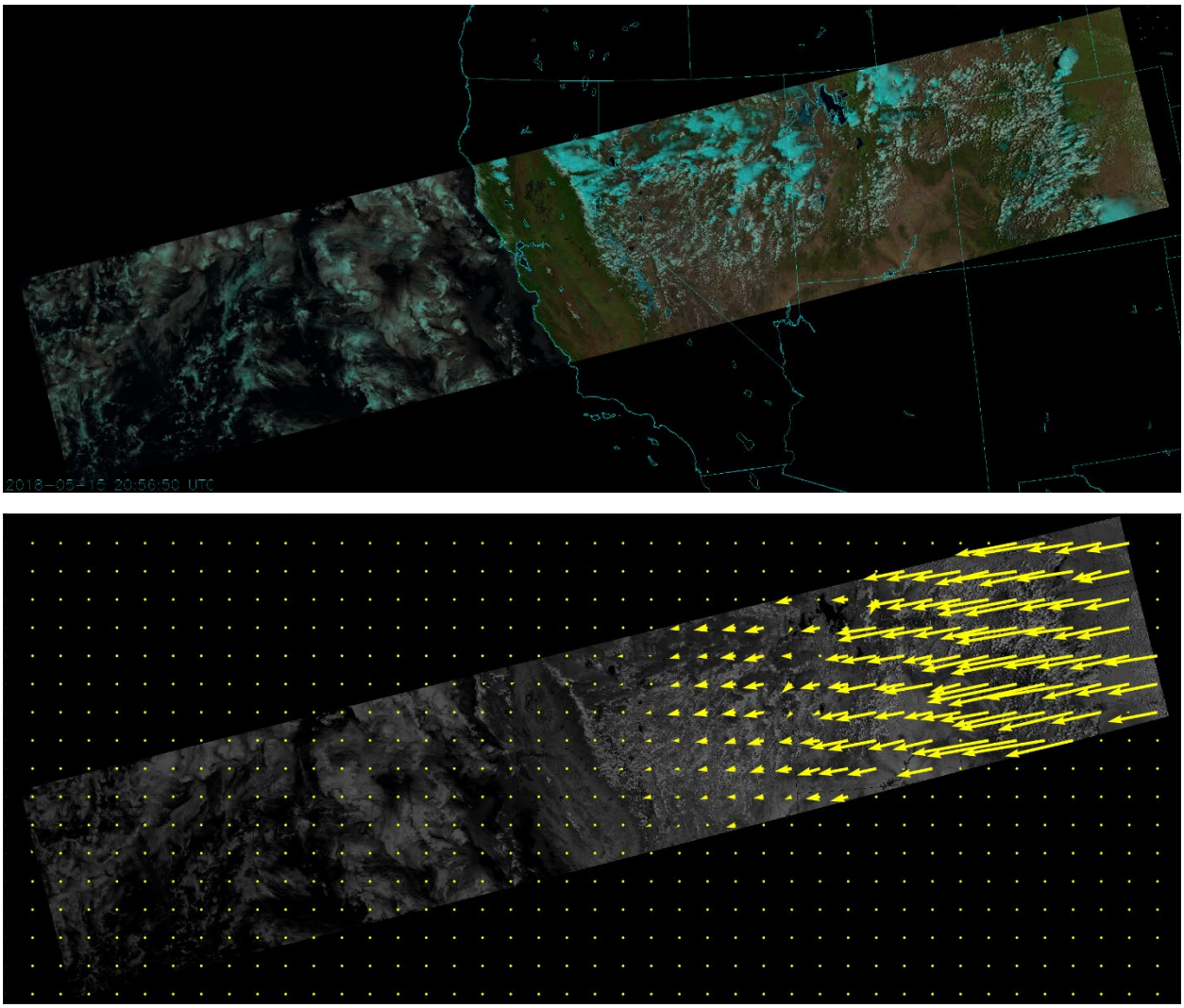

Figure 21. Image over the Rocky Mountains (on the right side of the VIIRS granule) from 15 May 2018, showing the degree of shift that occurs when TC is applied. The top image is an RGB using I-bands I3/I2/I1. The bottom image is the same granule for band I3 only with selected pixel shifts exaggerated for emphasis. Bottom image courtesy of J. Apke.

The image of this granule in its entirety reveals there is no shift either at nadir or on the entire west side of the same image, which lies over open water at sea level.

3.6 Algorithm Validation

The primary negative impacts to Imagery are usually found with the input SDRs, primarily calibration and geolocation considerations. These are validated by the VIIRS SDR Team. Since Imagery is fundamentally used in a qualitative manner, by a human analyst looking for features of interest, validation of the Imagery EDR focused on artifacts that would interfere with human interpretation of the Imagery EDR. The most common example of this is striping. However, the processing of the Imagery, to include the NCC process, was also necessary. Most of the early

analysis was manual inspection by Subject Matter Experts (SMEs), though this would often lead to more quantitative evaluation to determine a root cause.

The only issues noted shortly after the launch of SNPP was with the GTM process and fill values in the Imagery product tied to cross granule processing. The structure of the GTM grid was such that, near the edge of the granule, SDRs from pixels in the adjacent granule were required. If they were not available, an odd shaped triangle of fill would occur as shown in Figure 22. This granule was taken in the vicinity of New Zealand on 25 January 2012. The root cause of the fill data was determined not to be in the GTM processing but with so-called repair granules, a larger concern the program successfully addressed in mid-2012. The triangles no longer appear in the Imagery EDR output.

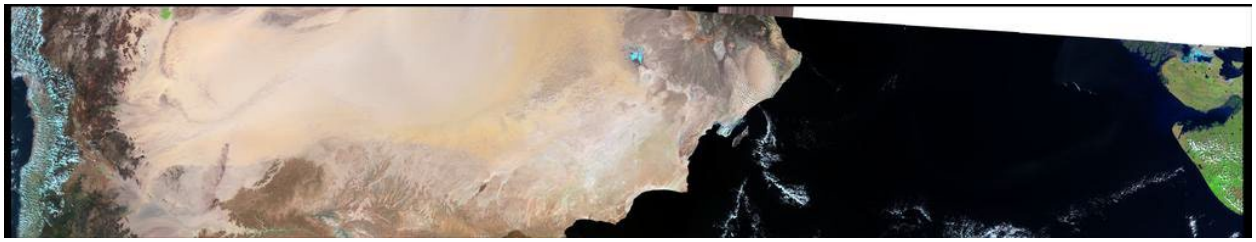

Figure 22. Imagery I-band 2 EDR from 25 January 2012. The white area in the upper right is all fill.

There were more issues with NCC. While the fundamental process of smoothing out gradients from solar/lunar illumination worked correctly, especially in the terminator region, multiple issues were noted with the nighttime NCC Imagery. During most of 2012, nighttime NCC Imagery was only producing a useful product when significant lunar illumination was available, that is with 72 hours either side of the full moon. Spotty fill values would grow in coverage until, by about half-moon lunar illumination, the entire product was fill. The subsequent investigation discovered that computation of pseudo-albedo exceeded prescribed limits when the base reflectance was very low. Hence the limits were widened from 0 to 5 and replaced with -10 to 1000 (negative numbers were necessary to account for negative DNB radiances in very dark pixels). Minor software changes were made and the GVVSSE and GVVSLE LUTs were recomputed. These steps fully resolved the issue. From the start, the daytime and terminator Imagery products have not exhibited any errors. Stray light in the NCC Imagery is addressed by corrections made in the DNB SDR.

The Imagery EDR User's Guide (Seaman et al, 2015) contains many examples of the Imagery EDR. The reader is invited to peruse that document for the many examples of Imagery EDR and related applications. Additional information can also be found in Hillger et al (2013). The program tracks all issues by writing and tracking Discrepancy Reports (DRs). There are no current open DRs regarding the performance of Imagery produced from VIIRS.

4 ASSUMPTIONS AND LIMITATIONS

4.1 Assumptions

There are only two assumptions that apply to the algorithms in this document. First, all reflectances and emittances for material classifications used in VIIRS simulations represent the real world. This first assumption applied to the algorithms when they were first developed, while VIIRS was still on the ground. The second assumption is the BRDF values are derived from the top-of-the-atmosphere radiance indicated in the Surface Reflectance Intermediate Product derived from VIIRS.

4.2 Limitations

The following limitations are applicable to the Imagery algorithms. The accuracy of any analysis derived from the Imagery EDR is tied to the resolution of the input SDRs. Sub-pixel features such as small cumulus clouds may not be detected by VIIRS. The same logic applies to any obscuration too thin to impact the VIIRS radiances (non-visible cirrus, small amounts of aerosols). In general, the defined limit of VIIRS sensitivity is an optical thickness of 0.03.

5 REFERENCES

Ackerman, S. A., K. Strabala, P. Menzel, R. Frey, C. Moeller, L. Gumley, B. Baum, C. Schaaf, and G. Riggs, (1997). Discriminating Clear-Sky From Cloud With MODIS Algorithm Theoretical Basis Document (MOD35). Version 3.2

Allen, R. C., P. A. Durkee, and C. H. Wash, (1990). Snow/cloud discrimination with multispectral satellite measurements. *J. Appl. Met.*, 29, 994-1004.

Arbeiter, R. (2008). Operational Algorithm Description Document for the VIIRS Ground Track Mercator (GTM) Imagery, EDR Software, D42815, Raytheon Company, pp 41.

Cao, C., X. (J.) Xiong, R. Wolfe, F. DeLuccia, Q. (M.) Liu, S. Blonski, G. Lin, M. Nishihama, D. Pogorzala, H. Oudrari, and D. Hillger, (2014). Visible Infrared Imaging Radiometer Suite (VIIRS) Sensor Data Record (SDR) User's Guide, *NOAA Technical Report NESDIS 142A*, 48 pp. https://www.star.nesdis.noaa.gov/smcd/spb/nsun/snpp/VIIRS/VIIRS_SDR_Users_guide.pdf

Data Dictionary for the VIIRS Imagery, (2015). Joint Polar Satellite System (JPSS) Algorithm Specification Volume II. 474-00448-02-26-B0200. https://jointmission.gsfc.nasa.gov/sciencedocs/2015-08/474-00448-02-26_JPSS-DD-Vol-II-Part-26_0200C.pdf

d'Entremont, R. P., Thomason, L. W. and J. T. Bunting, (1987). "Color composite image, processing for multispectral meteorological satellite data, *Proceedings of SPIE – The International Society for Optical Engineering*, pp. 96-106, Cambridge, MA.

Hillger D., T. Kopp, T. Lee, D. Lindsey, C. Seaman, S. Miller, J. Solbrig, S. Kidder, S. Bachmeier, T. Jasmin, and T. Rink, (2013). First-Light Imagery from Suomi NPP VIIRS. *Bull. Amer. Meteor. Soc.,* 94(7), 1019-1029, plus cover images. doi:10.1175/BAMS-D-12-00097.1

Hutchison, K. D. and A. P. Cracknell, (2006). VIIRS – A New Operational Cloud Imager, CRC Press, Taylor and Francis Group, ISBN-100-415-32129-8, pp 230.

JPSS-REQ-1001 Joint Polar Satellite Systems (JPSS) Program Level 1 Requirements – Final Version 2.0 (2016). http://www.jpss.noaa.gov/assets/pdfs/technical_documents/level_1_requirements.pdf

JPSS-REQ-1002 Joint Polar Satellite System (JPSS) Program Level 1 Requirements SUPPLEMENT – Final Version 2.10, (2014). http://www.jpss.noaa.gov/assets/pdfs/technical_documents/level_1_requirements_supplement.pdf

Liou, K-N. (1980). An Introduction to Atmospheric Radiation, Academic Press.

Scorer, R. S. (1990). Satellite as Microscope, Ellis Horwood Limited.

Seaman, C. (2013). Beginner's Guide to VIIRS Imagery Data. CIRA/Colorado State University. http://rammb.cira.colostate.edu/projects/npp/Beginner_Guide_to_VIIRS_Imagery_Data.pdf

Seaman, C., D. Hillger, T. Kopp, R. Williams, S. Miller, and D. Lindsey, (2015): Visible Infrared Imaging Radiometer Suite (VIIRS) Imagery Environmental Data Record (EDR) User's Guide, *NOAA Technical Report NESDIS 150*, 35 pp. doi.org/10.7289/V5/TR-NESDIS-150. ftp://ftp.library.noaa.gov/noaa_documents.lib/NESDIS/TR_NESDIS/TR_NESDIS_150.pdf

Thomas, G., and K. Stamnes, (1998). Radiative transfer in the atmosphere and ocean. Cambridge Atmospheric and Space Sciences Series.

Westinghouse Electric Corp. (1993). Technical Operating Report for Block 5D-3 Operational Linescan System (OLS) OLS 17-21.

6 APPENDIX: ACRONYMS USED IN THIS REPORT

AOT	Atmospheric Optical Thickness
ARF	Anisotropic Reflectance Factor
ARP	Application Related Product
ASGC	Along Scan Gain Control
ASP	Analog Signal Processor
ATBD	Algorithm Theoretical Basis Document
AVHRR	Advanced Very High Resolution Radiometer
BRDF	Bi-directional Reflectance Distribution Function
CCD	Charge Coupled Device
CCR	Configuration Change Request
CDR	Critical Design Review
CLASS	Comprehensive Large Array-data Stewardship System
CSPP	??
DMSP	Defense Meteorological Satellite Program
DNB	Day Night Band
DR	Discrepancy Report
EBBT	Equivalent BlackBody Temperature
ECR	Earth Centered Rotational
EDR	Environmental Data Record
DMSP	Defense Meteorological Satellite Program
DNB	Day Night Band
DoD	Department of Defense
GEO	Geolocation
GIFOV	Ground Instantaneous Field Of View
GMA	Gain Management Algorithm
GPS	Global Positioning System
GRAVITE	Government Resource for Algorithm Verification, Independent Test, and Evaluation
GTM	Ground Track Mercator
GVVSLE	Gain Value Versus Scene Lunar Elevation
GVVSSE	Gain Value Versus Scene Source Elevation
HIS	Horizontal Sampling Interval
HRI	Horizontal Resolution Interval

HSR	Horizontal Spatial Resolution
I-band	Imagery-resolution band
IDPS	Interface Data Processing Segment
IR	InfraRed
JPSS	Joint Polar Satellite System
KPP	Key Performance Parameter
LLLS	Low Level Light Sensor
LUT	Look Up Table
LWIR	Long-Wave InfraRed
L1RD	Level 1 Requirements Document
M-band	Medium-resolution band
MODIS	Moderate Resolution Imaging Spectroradiometer
MTF	Modulation Transfer Function
MWIR	Mid-Wave InfraRed
NCC	Near Constant Contrast
NGDC	National Geophysical Data Center (now NCEI)
NIR	Near InfraRed
NOAA	National Oceanic and Atmospheric Administration
NPP	NPOESS Preparatory Project (replaced by S-NPP)
NPOESS	National Polar-Orbiting Environmental Satellite System
NWS	National Weather Service
OLS	Operational Linescan System
RDR	Raw Data Record
RTM	Radiative Transfer Model
SBRS	Santa Barbara Remote Sensing
SDR	Sensor Data Record
SDSM	Solar Diffuser Stability Monitor
S-NPP	Suomi National Polar Orbiting Partnership
SNR	Signal-to-Noise Ratio
SWIR	ShortWave InfraRed
TDI	Time Delay Integration
TIROS	Television and InfraRed Observation Satellite
TOA	Top Of the Atmosphere
VDGA	Variable Digital Gain Amplifier
VIIRS	Visible Infrared Imaging Radiometer Suite
VNIR	Visible/Near InfraRed